Numerical Implementation of Crystal Plasticity Model for Face Centered Cubic Crystals

M.Tech Thesis

By

Mr. Harshdeep Sharma

DISCIPLINE OF MECHANICAL ENGINEERING

INDIAN INSTITUTE OF TECHNOLOGY INDORE

June , 2020

Numerical Implementation of Crystal Plasticity Model for Face Centered Cubic Crystals

A THESIS

Submitted in partial fulfillment of the
requirements for the award of the degree
of
Master of Technology

by

Mr. Harshdeep Sharma

DISCIPLINE OF MECHANICAL ENGINEERING
INDIAN INSTITUTE OF TECHNOLOGY INDORE

Candidate's Declaration

I hereby certify that the work which is being presented in the thesis entitled **Numerical Implementation of Crystal Plasticity Model for Face Centered Cubic Crystals** in the partial fulfillment of the requirements for the award of the degree of **Master of Technology** submitted in the **Discipline of Mechanical engineering, Indian Institute of Technology (IIT) Indore**, is an authentic record of my own work carried out during the time period from July, 2019 to July, 2020 under the supervision of Dr. Indrasen Singh, Assistant Professor in the discipline of mechanical engineering, IIT Indore.

The matter presented in this thesis has not been submitted by me for the award of any other degree of this or any other institute.

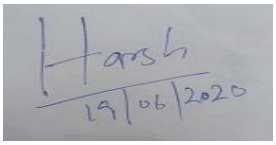

Signature of the student with date

This is to certify that the above statement made by the candidate is correct to the best of my/our knowledge.


19/06/2019

Signature of the Supervisor of
M.Tech. thesis (with date)

Mr. Harshdeep Sharma has successfully given his/her M.Tech. Oral Examination held on **25 June, 2020** .

Signature(s) of Supervisor(s) of M.Tech. thesis
Date:

Convener, DPGC
Date:

Signature of PSPC Member #1
Date:

Signature of PSPC Member #1
Date:

Acknowledgement

I begin by thanking my thesis advisor and mentor, Dr. Indrasen Singh, without whose guidance and encouragement this work would not have been possible. Discussions with him have always been educative. His work ethic is incredible and his guidance is the best one student aspires to get. He never fails to help his students in general even after being loaded with so much administrative works. He inspired and motivated me in all the walks of this work. I am very thankful to him in this memorable journey.

I am thankful to Prof. Pradeep Mathur, our Ex-Director, IIT Indore and our Current Director Prof. Neelesh Kumar Jain for giving an opportunity to carry out the research work and providing all the facilities.

I am also grateful to Prof. Eswara Prasad Korimilli for his guidance with respect to writing and presenting research work .

I also thank my colleagues in the lab Hirmukhe Sidaram, Ramanand Dadich, Prathamesh Powar and Anurag Sharma for their helpful suggestions time to time. All my lab mates have motivated me to work hard. Special thanks to Sir Hirmukhe for his help and care in all the way of this work. His excellence and knowledge in the field of Simulation works helped me a lot.

My special thanks go to my parents and my sister whose affection and constant encouragement has given me tremendous impetus in my academic pursuits. I once again thank all the amazing people who have made my stay at the institute one to cherish till eternity. Finally, I would like to bow to the Almighty, who is constantly helping me in achieving my aspirations in life.

Abstract

This study is focused to understand the deformation behavior of face centered cubic (fcc) metals through finite element simulations of tensile response of such materials. For this purpose, a physics based crystal plasticity model for fcc crystals which accounts for motion of dislocations and their influence on the plastic deformation is implemented in commercially available software package Abaqus 6.14 by writing material subroutine UMAT. The accuracy and performance of the numerical implementation is confirmed by comparing the predictions of tensile response from FE simulations with recent experimental data for single crystal Aluminum corresponding to wide range of temperature and strain rates. Computations are also performed to analyze the deformation response of single crystal Cu. Finally, the effect of applied strain rates and the orientation on crystals on the tensile response of Aluminum bicrystal is investigated.

Table of Contents

List of Tables

List of Figures

Acronyms

FCC	Face Centered Cubic
C3D8	Continuum Three-Dimensional Eight-Noded Solid Element
CPFEM	Crystal Plasticity Finite Element Method
FEM	Finite Element Method
RVE	Representative Volume Element
UMAT	User Materials Subroutine
a1	Coplanar Junction interaction coefficient
a2	Collinear Junction interaction coefficient
a3	Glissile Junction interaction coefficient
a4	Hirth Lock interaction coefficient
a5	Sessile junction interaction coefficient s
CRSS	Critically resolved shear stress
RSS	Resolved Shear stress
EBSD	Electron back scatter diffraction
HAGB	High angle grain boundary
LAGB	Low angle grain boundary
RD	Rolling Direction
TD	Tangential Direction
AD	Axial Direction

Chapter 1 Introduction

1.1 Introduction

The foundation of crystal plasticity can be traced back from the early 1900s (Taylor,1934). Orowan,1934 and Polyani,1934 also proposed that plasticity was due to the glide of dislocations, which are line defects on crystallographic slip planes. These slip planes together with the slip directions are specific for different crystal structures. Taylor in 1938 was the first to propose a theory for single crystal and polycrystal deformations based on the experiments done on Al single crystals and polycrystals (Taylor, 1923). He explained the polycrystal model by assuming the response to be homogeneous at the macroscopic level in each grain and proposed that the tensile behavior of polycrystals can be obtained from the tensile behavior of single crystal response. His assumption that each grain in the aggregate underwent the same homogeneous deformation satisfied the compatibility requirement by definition, however, the equilibrium of stress across at the grain boundaries were violated. The Taylor's model is rate independent one and the hardening across various slip systems is assumed to be isotropic i.e., all slip systems hardened at an identical rate which was a function of the total accumulated shear strain on all the slip systems.

It had already been established that any arbitrary strain in a polycrystal could be accommodated by just five independent slip systems in each grain (von Mises, 1928). The availability of more than five slip systems (i.e., twelve in an fcc metal) posed a non-uniqueness in the choice of active slip-systems. Taylor proposed that the active set was chosen in such a way that the net plastic work can be minimized. Though this reduced number of slip systems for the active set, there was still uncertainty about the choice of these active slip systems. Despite this ambiguity, his predictions for the macroscopic stress-strain behavior based on his model matched reasonably well with experimental observations.

Then in the latter half of the 20^{th} century the regime of the rate independent plasticity is extended by Asaro and Needleman (Asaro and Needleman, 1985). It laid to the entry in the new viscoplastic regime (Hutchinson, 1976). It is a power law kind of relation applies to materials

deformed via quasi-static strain rates under isothermal conditions. It is used for determining the shearing rate in each slip system unambiguously with the available variables of the slip resistance of slip systems and the driving force of plastic deformation. The validity of the Taylor-type model and its capabilities to predict texture evolution has been amply demonstrated with extensions to non-homogeneous, non-steady deformations (Bronkhorst et al., 1992) and modeling of complex metal-forming processes like rolling, deep-drawing etc (Chastel and Mathur, 1991 and Becker et al., 1993).

Flow rule signifies the condition when the plastic deformation will start but it is the hardening rule which determines the material behaviour with the continued deformation. As mentioned earlier, Taylor assumed an isotropic kind of hardening of the slip systems i.e, the hardening of the material is a function of one slip system only. This isotropic hardening model is unable to predict the experimental observation that inactive or latent slip systems often harden more than the slip system that is active during the deformation. Thus, in general as also revealed by the literature of the latter half of the 20th century (Peirce et al., 1982; Borja and Wren, 1993) the hardening is a function of slip on all the active slip systems.

This hardening of one active slip system due to plastic deformation in the other is called as Latent Hardening in the literature. The increase of flow stress as the material hardens is of the following form (Hill,1962):

$$\Delta g^{\alpha} = \sum_{\beta} h_{\alpha\beta} \Delta\gamma^{\beta};\ \alpha = 1, 2, \dots, N;\ \beta = 1, 2, \dots, N. \qquad \dots(1.1)$$

Here, the α and the β denotes different slip systems and $h_{\alpha\beta}$ is the associated hardening moduli of the slip systems. The diagonal terms in this hardening matrix refer to self-hardening while the off-diagonal terms refer to cross-hardening. Taylor's isotropic hardening rule implies that:

$$h_{\alpha\beta} = h;\ \alpha = 1, 2, \dots, N;\ \beta = 1, 2, \dots, N. \qquad \dots(1.2)$$

Other kinds of hardening models include independent hardening (Koiter,1953) which includes only the main diagonal terms and the models which include only off diagonal terms also known as Kinematic hardening models (Budiansky and Wu, 1962) where

$$h_{\alpha\beta} = hn^{\alpha}.n^{\beta};\ \alpha = 1, 2, \dots, N;\ \beta = 1, 2, \dots, N \qquad \dots(1.3)$$

where, n^{α} is the normal to yield's surface of the αth slip system .

Pierce, Asaro and Needleman, 1983 have used the following form of hardening (PAN Model,1983):

$$h_{\alpha\beta} = h(\gamma)\left(q + (1-q)\delta_{\alpha\beta}\right); \alpha = 1, 2, \dots, N; \beta = 1, 2, \dots, N. \quad \dots(1.4)$$

Where, $$h(\gamma) = h_0 \operatorname{sech}^2\left(\frac{h_0\gamma}{(\tau_s - \tau_o)}\right) \quad \dots(1.5)$$

where q is the latent hardening parameter $1 < q < 1.4$ (Kocks and Mecking ,1970) & h is the hardening rate at time t = 0 & τ_o and τ_s are the critical resolved shear stress at the time t = 0 and t = t_s at the saturation point & γ is the total accumulated slip strain.

Bassani and Wu [1991] have proposed a model for hardening in single crystals based on some careful experiments on copper single crystals in which the hardening modulii take the form:

$$h^{\alpha\alpha} = [(h_0 - h_s)\operatorname{sech}^2\left(\frac{h_0\gamma - h_s\gamma}{(\tau_s - \tau_o)}\right) + h_s][1 + \sum_{\beta=1,\beta!=\alpha}^{N} \tanh\left(\frac{\gamma^{\beta}}{\gamma^{\alpha}}\right) f_{\alpha\beta}] \quad \dots(1.6a)$$

and $h_{\alpha\beta} = \epsilon h^{\alpha\alpha}\ where, \epsilon \ll 1$ …(1.6b)

where τ_s is the stage I strength, i.e., the breakthrough stress level at which large plastic flow starts & h_0 and h_s, define the hardening slope after the initial yield and during easy glide, respectively & ϵ is a small parameter which defines the off-diagonal terms and is an interaction matrix that depends on the nature of the junctions formed between slip systems α and β. Wu, Bassani and Laird , 1991 argue that the activation of secondary slip during stage II deformation before tensile overshoot, is inconsistent with the notion of strong latent hardening during single slip for most crystal orientations. They hypothesized the experimental results by concluding that a very small latent hardening but high active hardening rate on latent systems. This, they claim, has been overlooked owing to the back-extrapolation methods used to estimate the critical resolved shear stress. Bassani in 1993 has proposed a hardening form to include the effects of stage III hardening by assuming that h, depends on the total accumulated slip on all systems as the following form:

$$h_s = h_s^I + (h_s^{III} - h_s^I) \tanh\left(\frac{\gamma}{\gamma_0^{III}}\right) \quad \ldots(1.7)$$

where γ_0^{III} is the accumulated slip at the onset of stage III of plastic deformation & h_s^I and h_s^{III} are the hardening modulii at the beginning of easy glide and stage III deformation respectively. Other forms of Hardening law as those given by Kalidindi, Bronkhorst and Anand [1992] are available too in the literature but many researchers to date use the hardening law of Pierce et. al and Bassani's law to simulate the BCC, FCC and even HCP metals as well both single crystal and polycrystalline materials as well.

1.2 Brief outline of the work

Plasticity of crystalline materials is inherently rate – dependent. Most of the fcc metals viz, Aluminium and Copper hardens at higher rate as we increase the rate of deformation (Khan et. Al, 2015) and (liu , 2008) . Plasticity is also temperature dependent and is Orientation dependent too (Anisotropic). Hence, there is a need to have the constitutive law for slip based on these aspects. Such a form would not only be more physically based but also dispense with the issues of non-uniqueness of solutions encountered in the rate-independent framework. The slip-system hardening laws are crucial in predicting observed phenomena such as premature secondary slip, tensile overshoot, etc. in single crystals of BCC metals, though these are not very critical in polycrystals deformations. Finally, there is a need to implement the developed models in hand and measure their success in predicting the tensile response of Aluminum bicrystals after matching them with the experimental results. In the present study, a rate and temperature dependent single-crystal plasticity model has been outlined which is more physics based viz, density of the dislocation. The framework for the constitutive model based on the work of Huang [1991] and Khan et al (2015) is presented in Chapter 2 in which we discussed the slip based on thermally activated motion of dislocations PAN et al , 1983 and Bassani et al , 1991 hardening form is also discussed in this rate-dependent framework. The predictions for tension of single crystal pure (99.99%) Aluminum and copper are benchmarked with the available results of the literature. The implementation of the work discussed in the Chapter 2 is discussed in Chapter 3

on Aluminum bicrystals which can be further extended to the polycrystalline materials . Predictions of the model for different rate of deformation and their comparison with experiments are also shown. The capabilities of the model of texture evolution is also discussed in the same chapter. The conclusions and the future scope of the work is summarized in Chapter 4. In the next sections we will discuss about what are the various slip systems in the face-centered cubic metals how one can represent those and also, we will discuss some of the industrial applications of these metals.

1.3 Fundamental aspects of Face Centered Cubic metals

1.3.1 Slip systems

Slip Systems are the combinations of slip planes also knows as dense planar surfaces and slip directions also known as directions of plastic deformation and directions of dislocation motion. We will discuss more about dislocations (line defects in the crystalline materials) and their motions in the subsequent sections.

Let us define the dense planes of a crystal structure, as the ones at which the denser possible arrangement of atoms (spheres) is achieved. Subsequently, we also define the directions along which the atoms are sorted in the denser possible manner as dense directions. In most dense crystal structures, atoms osculate along dense planes and directions. It should be noted however, that dense planes and directions are typical of the specific structure since they depend on the exact atom arrangement. For instance, planes of the {111} plane family are the dense planes and crystallographic directions < 110 > are the dense directions of the FCC structure as shown in the following figure. On the other hand, the dense planes of the BCC structure are the {110} whereas their dense directions are the < 111 >.

The combination of slip planes normal and directions in the sense {abc} < hkl > defines the structure's slip systems. Slip systems are greatly important to the plasticity of metal single crystals, since atomic slip can only occur along slip directions located on slip planes. The latter also justifies the fact that dense directions are also commonly referred to as slip directions, whereas dense planes as slip planes. FCC metals contain 12 {111} < 110 > slip systems the relative position of slip planes normal and directions forming the slip systems of FCC crystals is schematically illustrated in Figure 1.1

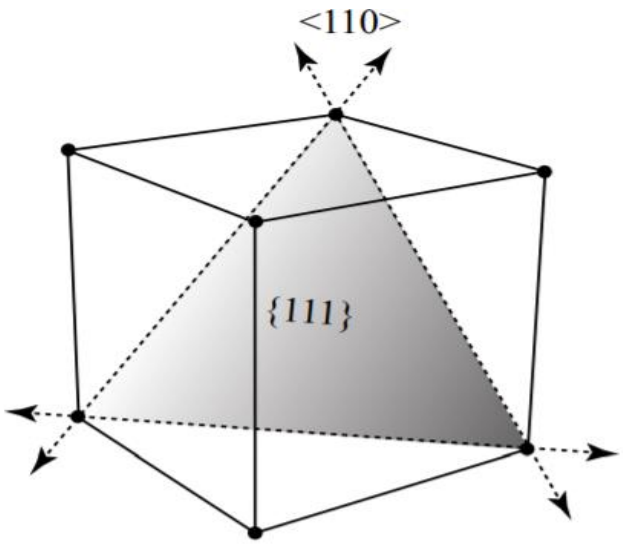

Figure 1.1 : Schematic showing the slip planes (dense planes) and line directions of maximum linear density of atoms for Face Centered Cubic metals .

1.3.2 Dislocations and its types

Dislocations are the most important subset of defects in crystalline solids therefore an elementary understanding of dislocations and their types and also their motion is required. Although there are many techniques available to directly observe dislocations, the existence of dislocation (line defects) was assumed during early studies when unexplained discrepancies arose between the theoretical and experimental values of applied shear stress to deform a single crystal. This deformation occurs by the sliding of atomic planes, and in a perfect crystal, the rigid movement of all atoms simultaneously. First calculations of the required shear stress to impose this deformation were by Frenkel in 1926. The theoretical maximum or critical value of shear stress (τth) was found to be many orders of magnitude greater than the experimentally obtained values.

Orowan (1934), Polanyi (1934), and Taylor (1934) independently were able to account for this by the presence of dislocations.

The most useful definition of a dislocation is given in terms of the Burgers circuit. A Burgers circuit is a planar closed loop atom-to-atom path. If the circuit encloses a dislocation, it does not close due to an atomic mismatch and the vector required to close the circuit is known as the Burgers vector. Two important rules regarding edge and screw dislocations are as follows: (i) the Burgers vector of an edge dislocation is perpendicular to the line of dislocation and (ii) the Burgers vector of a screw dislocation is parallel to the line of dislocation.

1.3.2.1 Edge dislocations

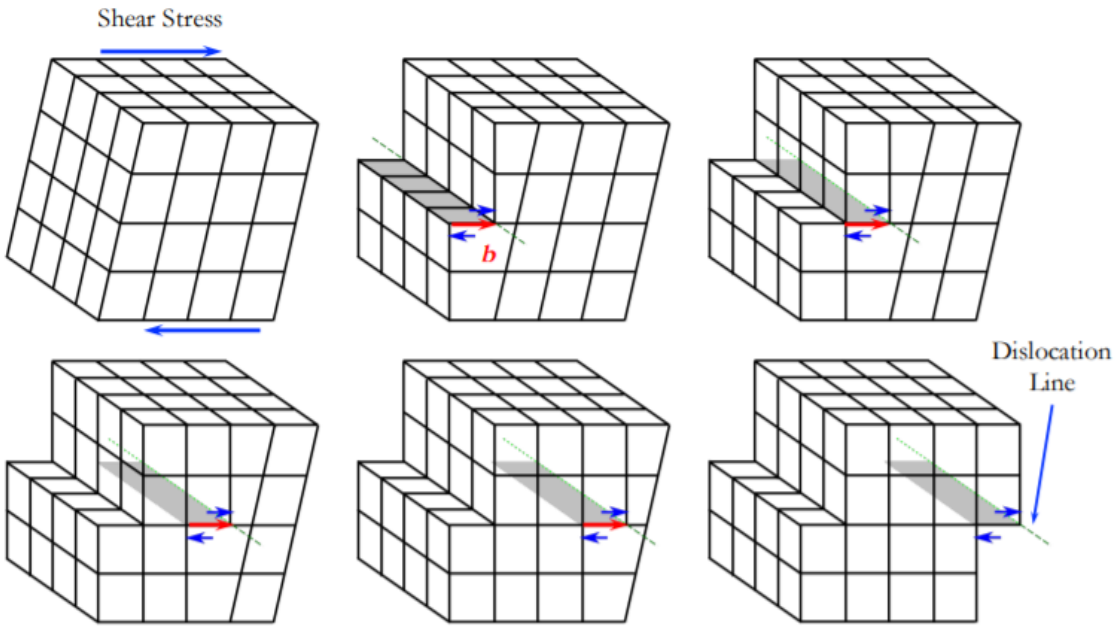

Figure 1.2a) Edge dislocation propagation through a crystal lattice with Burgers vector ***b*** *(Hull and Bacon,2001).*

In an edge dislocation, the dislocation propagates along the line of the applied shear stress. In a screw dislocation, the atoms 'twist' propagating the dislocation line perpendicularly to the applied stress. In the example below both types of dislocation yield the same final deformation after the dislocation has completely passed through the crystal.

1.3.2.2 Screw dislocations

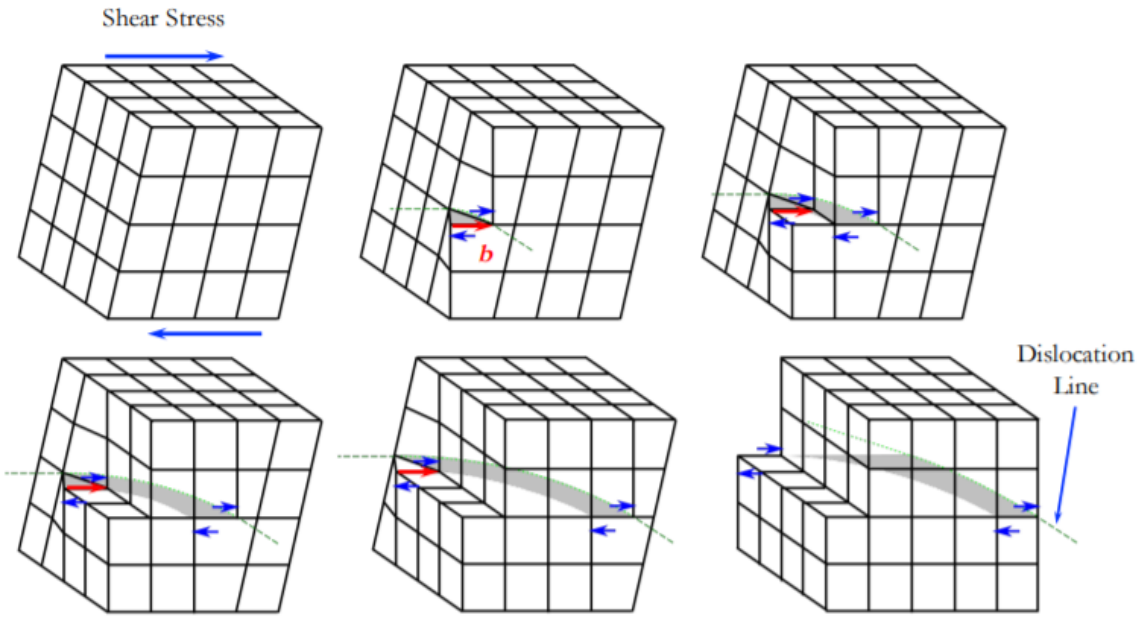

Figure 1.2b) Screw dislocation propagation through a crystal lattice with Burgers vector ***b*** *(Hull and Bacon, 2001).*

1.3.2.3 Mixed dislocations

In general, pure screw and pure edge dislocations are rare in crystalline materials and the dislocations in general have been observed experimentally as dislocation loops containing edge and the screw component as shown in the Figure 1.2c). Dislocation channels containing lot of dense dislocation loops have been seen after irradiating a surface with nuclear radiation as seen on the nuclear cladding. Dislocations motions are the primary source of plastic deformation in crystalline materials and it is been seen even more pronounced when the material enters the plastic regime while undergoing continuous deformation.

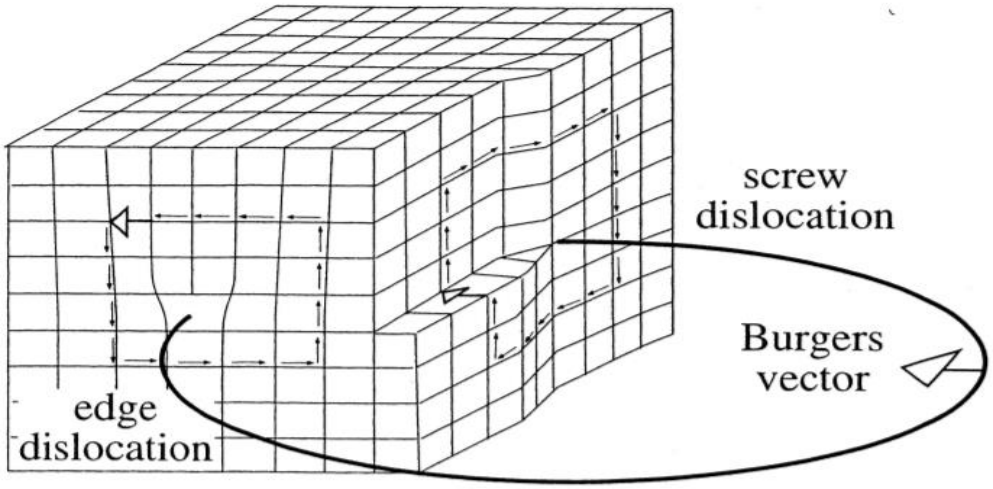

Figure 1.2c) Mixed dislocation containing both the edge and the screw component (Hull and Bacon, 2001).

1.3.3 Dislocation motion

There are two basic modes of dislocation movement: glide and climb. Dislocation glide is when the dislocation motion, line, and Burgers vector all shares the same plane. This is also known as conservative motion and when many dislocations glide, the results is slip, which is the most dominant manifestation of plastic deformation in crystalline solids such as aluminum. Climb, or non-conservative motion, occurs when the dislocation motion is out of plane and normal to the Burgers vector.

1.3.3.1 Dislocation Glide

A characteristic shear stress is required for slip to occur. For example, in Figure 1-3 a crystal is deformed under tension by an applied force F along the axis of the cylinder. Assuming the cross sectional area to be A, the stress developed parallel to the applied force is $\sigma = F/A$. This force has a component in the slip direction $F\cos\lambda$ with λ being the angle between F and the slip direction. This force component acts over the slip surface with an area $A/\cos\phi$, where angle ϕ is the

rotation from F to the slip plane normal. Therefore, the resolved shear stress on a given slip plane and given slip direction can be represented as

$$\tau = (F/A)cos\lambda cos\phi \qquad \ldots(1.8)$$

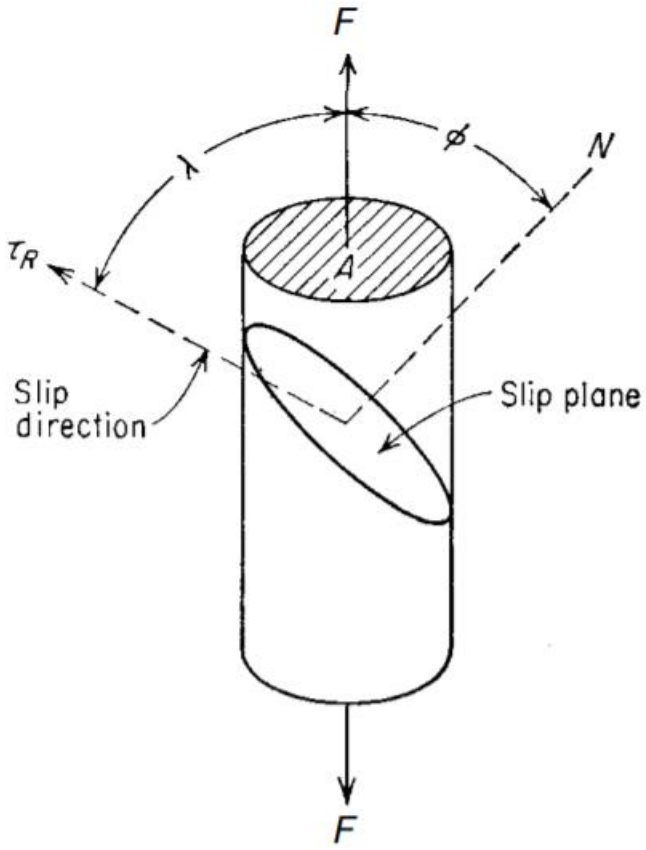

Figure1.3) Geometry of slip in crystals and In general, (λ + ϕ) ≠ 90˚.

Throughout this work, τ is used to represent the shear stress resolved on to a slip system in this way. Furthermore, if a critical force F_c is required to initiate slip, the corresponding shear stress is denoted τ_c or critical resolved shear stress (CRSS). The translation cosλcosϕ from σ to τ is known as the Schmid factor.

Dislocations move by glide at a velocity dependent on the magnitude of the applied shear stress, the purity of the crystal, temperature, and the type of dislocation. A method of measuring dislocation velocities developed by Johnson and Gilman found that in the range of 10^{-9} to 10^{-3} ms^{-1} , the logarithm of the dislocation velocity was linearly proportional to the logarithm of applied stress, such that

$$v_{disl} = \left(\frac{\tau}{\tau_0}\right)^n \quad \ldots(1.9)$$

where τ is the applied shear stress and τ0 is the shear stress such that v_{disl} = 1 ms^{-1}, and n is a proportionality constant. It should be noted that, the above relation is purely empirical, with no implied physical interpretation of dislocation motion mechanisms.

At low temperatures diffusion is extremely difficult and the movement of dislocations is nearly entirely restricted to dislocation glide. However, at elevated temperatures where thermally motivated diffusion is active, an edge dislocation can move out of its slip plane through a mechanism called dislocation climb.

1.3.3.2 Dislocation Climb

Physically, climb is the diffusion individual, or clusters, of vacancies toward or away from the dislocation. The result of dislocation climb is what is known as a jog and only occurs on edge dislocations (Hirth and Lothe, 1982).

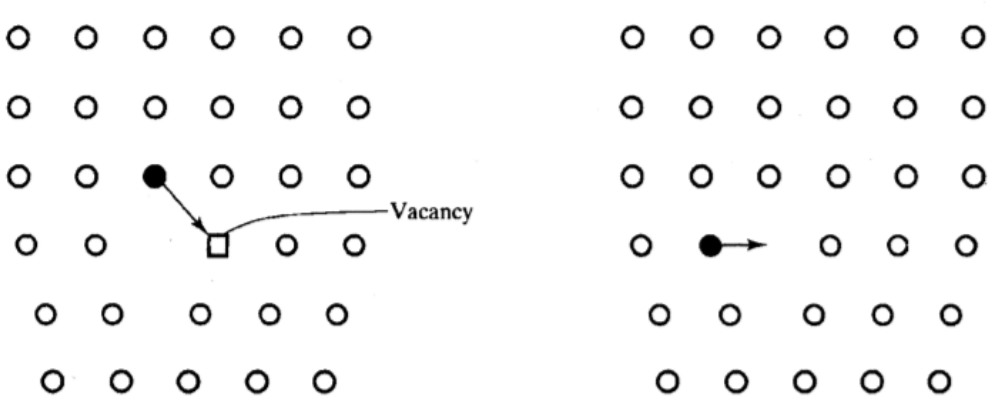

Figure 1.5: (a) Schematic showing the mechanism of dislocation climb by interchanging atoms along its core with the adjacent vacancy .(b) Mechanism of reverse climb where an atoms leaves its site to enter into the dislocation core leaving behind lattice vacancy (T.Courtney,1990).

All of these factors play an important role in work hardening, especially in dislocation dominant materials such as aluminum. When dislocations move, interact, and change their distribution or density in the material, the glide resistance increases. For almost all metals, this has been used as

an improvement to the material by increasing the strength through plastic deformation. The first work in realizing the connection between dislocation interactions and work hardening was completed by Taylor (1934). Taylor proposed the shear stress that is required to move two parallel plane edge dislocations separated by l past each other to be

$$\tau = \alpha \mu b / l \qquad \ldots(1.10)$$

where α is a constant of order 0.1 related to the strength of obstacles in the matrix, μ is the shear modulus, and b is the Burgers vector. The average dislocation spacing l is proportional to the inverse root of the dislocation density, i.e. $l \approx \rho^{-1/2}$. Taylor extended this to a parabolic relation for stress-strain, which decently fits the behavior of many polycrystalline materials; however, single crystals may not behave in the same manner (Taylor, 1934).

Chapter 2 Review of pertinent literature

2.1 Introduction

In the first chapter, we begin our journey by discussing the fundamental aspects of FCC crystals deformation mechanism and it turns out to be that these deformation mechanism can turn out to be complicated interaction within a crystal i.e., interaction of dislocation with another dislocation (edge or screw dislocation) ; interaction of dislocation with an impurity or precipitates which are typical existence within a crystalline material ; interaction of dislocation with a void (volumetric defects) , a vacancy (point defects) & Grain boundaries(HAGB and LAGB) etc. etc. However, among all the interactions if we talk about the single crystal then the interaction of dislocation with another dislocation is the most important and decisive one so, thus we will discuss now various stages of plastic deformation reported in the literature and how the latter interaction plays the significant role in it and in this way we will dive into the existing literature to conclude with the formulation of the work statement of our study .

2.2 Plastic deformation of single FCC crystal

The typical shear stress-shear strain response for a single crystal is illustrated in Fig.2.1. The response is elastic till a threshold value of shear stress τ_0, is reached. Thereafter, the τ -γ curve is divided into three regions of easy glide, linear hardening and dynamic recovery or parabolic hardening (referred to as stages I, II and III, respectively).

Initially, slip occurs on a single plane, and the rate of strain hardening is very low. This low strain hardening rate is similar to that in crystals of HCP metals and is called easy glide or stage I. At some point, slip is observed on other systems. The result is that dislocations on different slip systems intersect, causing much more rapid strain hardening. Dislocations multiply rapidly in this stage and interact with each other to form various kind of locks (e.g., Hirth lock, Lomer-Cottrel lock, etc.). Consequently, there is dramatic increase in the rate of hardening h_{II} . Lower temperatures increase the extent of stage II. Stage III is a region of decreasing rate of strain

hardening (i.e., parabolic hardening) because of cross-slip of dislocations. It is important to note that hardening of a particular slip system may occur due to slip on other systems.

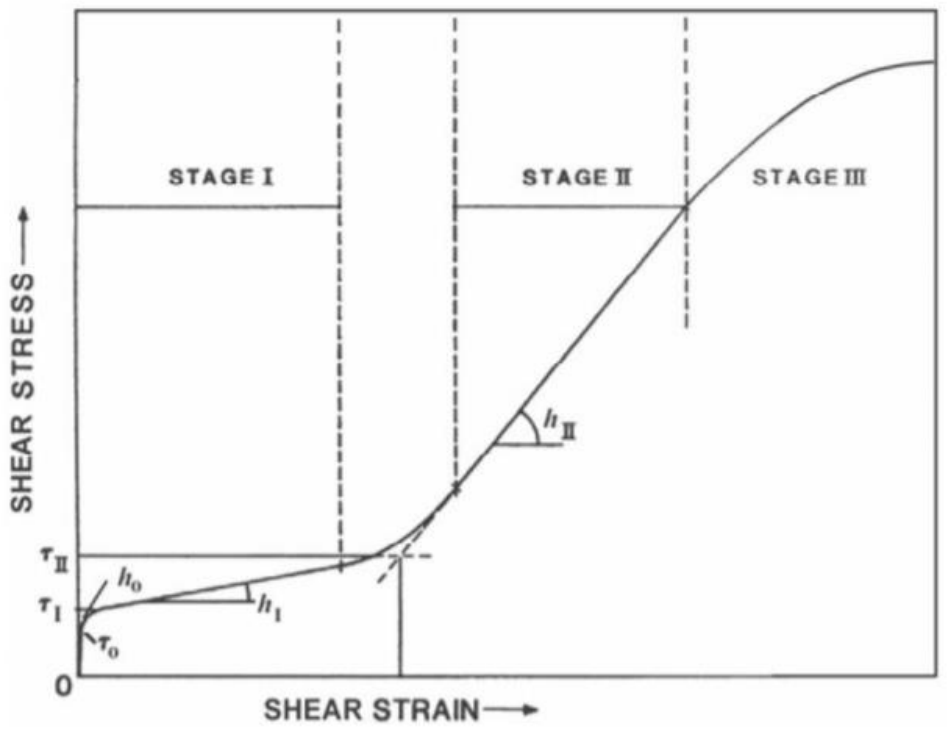

Figure 2.1 Schematic showing various stages of work hardening typical of FCC single crystal under shear (Swapnil thesis,2009)

The extent of easy glide in a crystal depends on its orientation, its perfection, and the temperature. A high degree of crystal perfection and low temperature promote easier glide. Likewise, the extent of easy glide is greater in orientations for which the resolved shear stress on other potential systems is low. Easy glide does not occur in fcc crystals oriented so that slip occurs simultaneously on many slip systems. Late stage IV, V and VI have been identified at large strains (Argon and Haasen, 1993; Les et al., 1996, 1997; Mecif et al., 1997). The existence and extent of each stage depend on many factors such as the initial crystal orientation, temperature and strain rate and the type and purity of metal.

2.3 Crystal Plasticity Models for FCC metals

Various plasticity theories have been proposed to predict the deformation response of FCC metals, which are divided in different categories. They are briefly reviewed under respective category in the following.

2.3.1 Category I Models (e.g. Taylor's Model[1938])

An early, and pioneering, attempt at this problem was made by Taylor (1938). He calculated the global stress response of a strain rate independent FCC polycrystal, assumed to be rigid-plastic, subject to an increment of tensile strain. He further assumed that each grain (or single crystal) of the polycrystal was subject to the same uniform deformation as was the entire aggregate. This calculational procedure has come to be generically known as the Taylor model, and is currently widely used to predict the development of deformation textures and the constitutive behavior of polycrystals subject to large strains (see, e.g. Bishop, 1954 ; Dillamore and Katoh, 1974 ;Gil Sevillano, Van Houtte and Aernoudt,1980). But these kind of models fails in the sense that when it is seen experimentally by many experimentalists (Taguchi,1974) on Cu single crystals and many other that plasticity is inherently rate and temperature dependent .Before coming to the latter models, it is worth mentioning that Taylor kind of model also fails in the sense that it had also been observed localized and non- uniform plastic deformation on ductile single crystals subjected to tensile loading and so we come to the second kind of models .

2.3.2 Category II Models (e.g. PAN Model [1982])

The work of Pierce, Asaro and Needleman is numerical one and they showed the importance of latent hardening and that defies the Taylor's approximation of isotropic hardening. Their calculations follow the crystal through necking and the formation of shear bands and describe several important features of shear localization which are in close agreement with experiments as shown in the Figure 2.2 i.e., the material planes of the bands are found to be inclined at a characteristic angle to the slip plane orientation. As a consequence of material compatibility, lattice rotations occur. These rotations cause geometrical softening of the bands: i.e. the higher valued resolved shear stress. The computed lattice rotations are in close correspondence with

those found experimentally. The limitations of this kind of models is also like the Taylor kinds of models is the inability to capture rate effects .

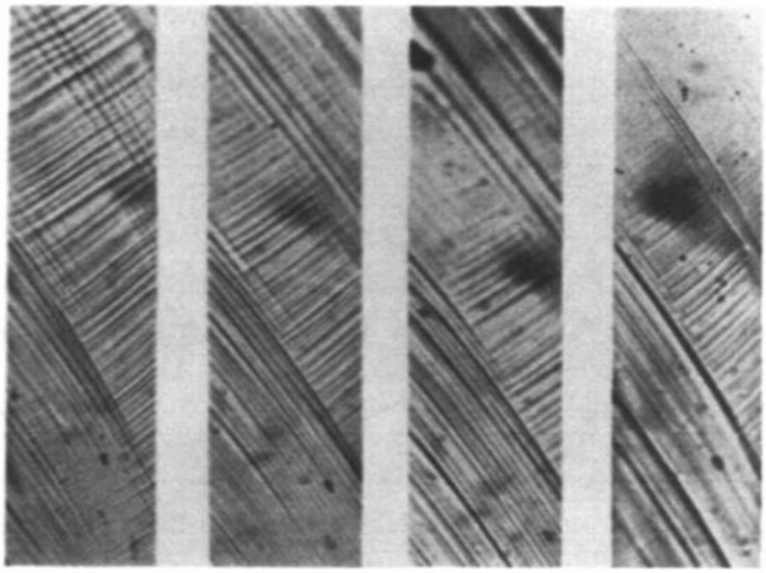

Figure 2.2 Photograph showing gage section of α brass taken from the works of Pierce et al.

2.3.3 Category III Models (e.g. PAN model type II [1983])

Pierce et al. Model II mentions about the limitations of the rate independent framework and it said that the limitations are so severe that to cover full range of material properties it is customary to include the rate dependence in the constitutive framework .Later on other models of Harren et al. (1982,83) Becker et al. (1991,92) were also on the similar trajectory as the foundation laid by PAN model II . Dislocation slip is the main deformation mechanism and slip resistance strength is the only internal state variable so these kinds of models are not physics based and more or less are mathematical kind and also they do not capture strain rate effect over a wide range of strain rate viz , from quasi static to more dynamic range .

2.3.4 Category IV Models (e.g. Nemat-Naseer et al.[1998])

In 1998 , Based on the results of a series of experiments on commercially pure OFHC (oxygen free high thermal conductivity) copper (an FCC polycrystal), a physically based, rate- and temperature-dependent constitutive model was proposed for FCC single crystals. Using this constitutive model and the Taylor averaging method, numerical calculations were performed to

simulate the experimental results for polycrystalline OFHC copper. This model calculation is based on a new efficient algorithm which had been successfully used to simulate the flow stress of polycrystalline tantalum over broad ranges of temperature, strain rate, and strain (Nemat-Nasser, S., Okinaka, T., Ni, L., 1998). This model effectively simulates a large body of experimental data, over a broad range of strain rates (0.001 to 8000 s^{-1}), and temperature (77K to 1096 K), with strains close to 100%. Few adjustable constitutive parameters of the model were fixed at the outset for a given material. This kind of models was a success among all its predecessors and eventual successors too but the only small limitations of this kind of models and other models of Balasubramanian and Anand (2002) & Hansen et al. (2013) etc. etc. is that the more complex phenomenon of dislocation motion causing complex interaction among themselves is not properly understood .Moreover the internal state variable is also not based on the physics of slip rather it is the slip resistance strength which in itself need to be explored.

2.3.5 Category V Models (e.g. M.G. Lee [2010])

Single crystal constitutive equations based on dislocation density (SCCE-D) were developed from Orowan's strengthening equation and simple geometric relationships of the operating slip systems. The flow resistance on a slip plane was computed using the Burger's vector, line direction, and density of the dislocations on all other slip planes, with no adjustable parameters. That is, the latent/self-hardening matrix was determined by the crystallography of the slip systems alone.

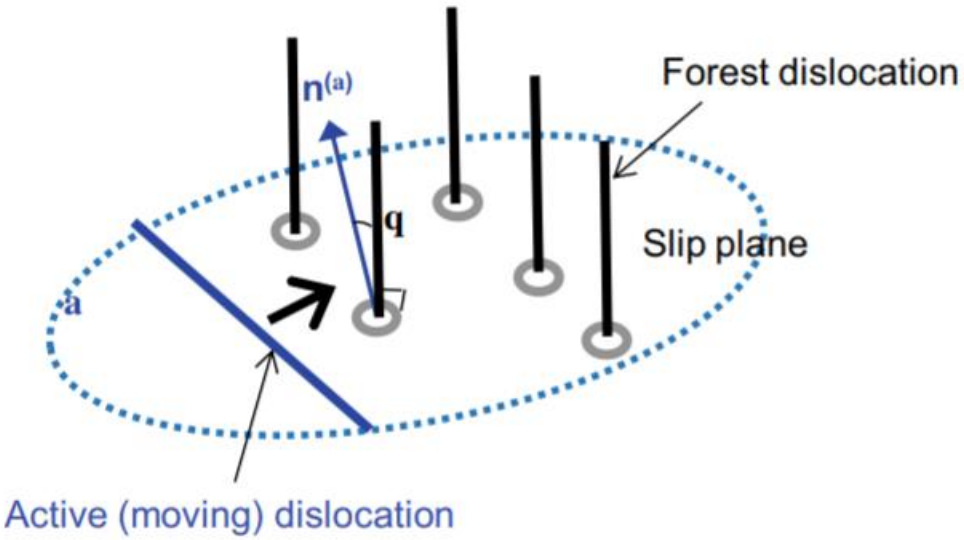

Figure 2.3 Interaction of a moving dislocation with an array of immobile (forest) dislocation (M.G.lee ,2010)

This models are more realistic models and misses the thermally activated flow rule of plasticity and other predecessors like Kocks and Mecking (2003) & Beyerlinand Tome (2008) were based on the similar frameworks as well .

2.3.6 Category VI Models (e.g.Kubin and Estrin[1990])

More physical and advanced models includes those that separate the mobile and forest dislocations (Kubin and Estrin, 1990; Barlat et al., 2002; Austin and McDowell, 2011; Hansen et al., 2013), those that separate the edge and screw dislocations (Arsenlis and Parks, 2002; Alankar et al., 2009), those that consider the development of the dislocation densities in cell walls and grain interiors (Estrin et al., 1998; Roters et al., 2000; Tóth et al., 2001) and those consider the geometrically necessary dislocations (GND) in addition to the scalar statistically stored dislocations (SSD) (Ma and Roters, 2004; Ma et al., 2006a, 2006b; Gurtin, 2010).

It is worth mentioning that as the complexity of models increases, the number of parameters that need to be identified also increases and it is usually more difficult to perform the numerical simulations.

2.4 Challenges involved in the development of CPFEM model

- ➔ Development of Algorithm: It involves complex interaction taking place at the microstructural level e.g. slip, twinning and their interaction
- ➔ Hardening models: Due to the paucity of information Dislocation evolution and their complex interactions selection of right hardening model is always challenging
- ➔ Selection of integration scheme: Conventional numerical integration techniques such as Newton Raphson or return mapping schemes doesn’t converge ; Modified schemes have to be employed

2.5 Issues needs to be addressed

- ➔ Commercial packages like Abaqus, Marc, Ansys does not include the CPFEM models.
- ➔ Every group develops their own user subroutine and does not share the information with others. So limited information is available about any specific CPFEM model.
- ➔ One has to develop their own Algorithm to adopt for their research.

2.6 Objectives

Based on the issues identified in the above the objectives for the present thesis are framed as:

- ➔ To implement CP model for FCC single crystal by writing subroutine UMAT in commercially available software ABAQUS.
- ➔ To benchmark the developed UMAT against the experimental results available in the literature. In the present study we benchmark it against the experimental results of Pure Al carried out by Khan et al.(2015) under a wide range of strain rate (0.001-$10^3 s^{-1}$) and under different - different orientation w.r.t. the tensile loading direction.
- ➔ To study the plastic deformation of aluminum bicrystals under different – different orientations and also under a wide range of strain rate (same range as above) and see how the orientation of one crystal and the other crystal effects the plastic deformation and analyze the contour plot closely .

Chapter 3 Numerical formulation and Implementation of the Crystal Plasticity Model for Face Centered Cubic single crystal

3.1 Introduction

In this chapter, the general framework of crystal plasticity finite method (CPFEM) theory is presented . The detailed derivation of the modeling equation to be finally incorporated in the user material subroutine in ABAQUS is done in the following sections. The fundamental aspects of CPFEM theory is invariant and various models differs only in their mechanism-based modeling equations.

The deformation mechanism in this study is based on the dislocation glide which is the primary deformation mechanism in the face centered metals at room temperatures .The effects of twinning, martensitic transformation etc. is not taken into consideration which are very low temperature based or very high temperature based mechanisms. The effect of loading rate and the effect of orientation is implicit in the derivation of the model.

3.2 Numerical Formulation of CP model

3.2.1 Kinematics

The kinematics of crystal plasticity has been developed by Hill (1966), Rice (1971), Hill and Rice (1972), and Hill and Havner (1982). Reviews and references are given by Havner (1992). The geometrical shape deformation of a crystal can be mathematically decomposed into the elastic and plastic part as:

$$F = F^{*}F^{P} \qquad \text{…..(3.1)}$$

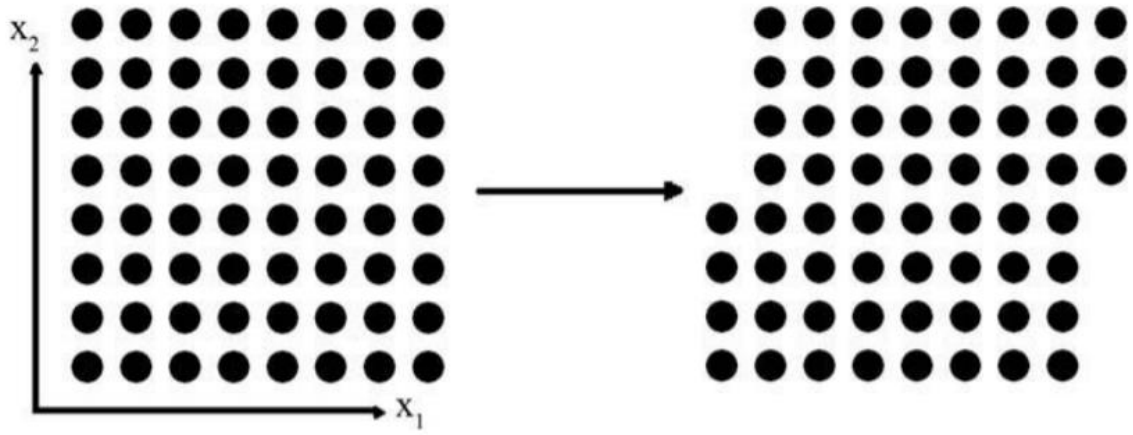

Figure 3.1 Schematic illustration of pure plastic deformation $F = F^{P}$ (Raabe et al.[2010])

In Fig. 3.1 the crystal lattice is unchanged in the reference and current states, so all the work expended in the process is dissipated as heat and the material remains in the same thermodynamic state before and after the deformation. At the end of the process the external loads can be removed and no lattice deformation remains, $F = F^{P}$

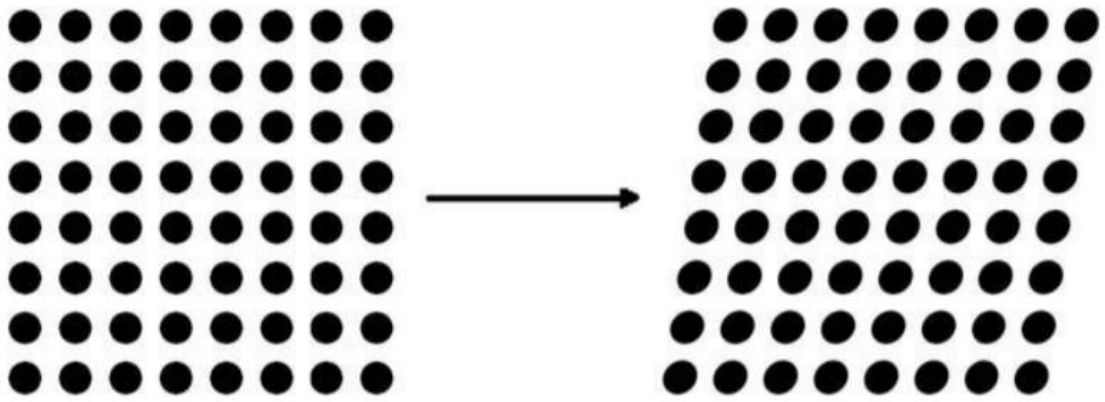

Figure 3.2 Schematic illustration of pure lattice rotation $F = F^{*}$ (Raabe et al.[2010])

In contrast, the crystal undergoes an purely elastic shape change in Fig. 7. In this case there are no dislocations, the lattice is distorted congruently with the external shape of the body, $F = F^*$, and the external cause for the deformation must be maintained in order to preserve the change in shape; removal of the external boundary conditions causes the body to revert to the reference state. Also the thermodynamic states of the reference and current states are different because of the stored elastic energy due to the lattice deformation.

In total the deformation is said to take place in a way that firstly F^P brings the crystal from reference configuration to the intermediate configuration and then finally F^* brings the crystal from the intermediate configuration to the final configuration thus thereby, completing the entire shape change and in the process of the rotation the inherent slip systems rotate as well according to the basic transformation law of vectors and tensors as:

$s^{*\alpha} = F^* s^\alpha \quad , \quad m^{*\alpha} = F^{*-T} m^\alpha$ … (3.2)

The form of $m^{*\alpha}$ is chosen such that in the current configuration $s^{*\alpha}.m^{*\alpha} = s^\alpha.m^\alpha = 0$

By definition the velocity gradient is written as:

$l = \dot{F}F^{-1} = \dot{F}^* F^{*^{-1}} + F^* \dot{F}^P F^{P^{-1}} F^{*^{-1}}$ … (3.3)

Further simplification gives, $l = L^* + F^* L^P F^{*^{-1}}$ … (3.4)

Since $L = \left(\frac{1}{2}\right)(L + L^T) + \left(\frac{1}{2}\right)(L - L^T)$ …(3.5)

$= D + \Omega$

Flow rule , $L^P = \dot{F}^P F^{P-1} = \sum_{\alpha=1}^{n} \dot{\gamma}^{(\alpha)} \left(s^{(\alpha)} \otimes m^{(\alpha)}\right)$ (Asaro et al.[1983]) …(3.6)

Further the unit symmetric and anti-symmetric tensor along the flow rule is given as:

$\mu_{ij}^\alpha = 1/2\left(s_i^{*\alpha} m_j^{*\alpha} + s_j^{*\alpha} m_i^{*\alpha}\right)$ …(3.7)

$\omega_{ij}^\alpha = 1/2\left(s_i^{*\alpha} m_j^{*\alpha} - s_j^{*\alpha} m_i^{*\alpha}\right)$ …(3.8)

Further the full symmetric and anti-symmetric component is given as follows:

$D_{ij} - D_{ij}^* = \sum_\alpha \mu_{ij}^\alpha \dot{\gamma}^\alpha$ ….(3.9)

$\Omega_{ij} - \Omega_{ij}^* = \sum_\alpha \omega_{ij}^\alpha \dot{\gamma}^\alpha$ ....(3.10)

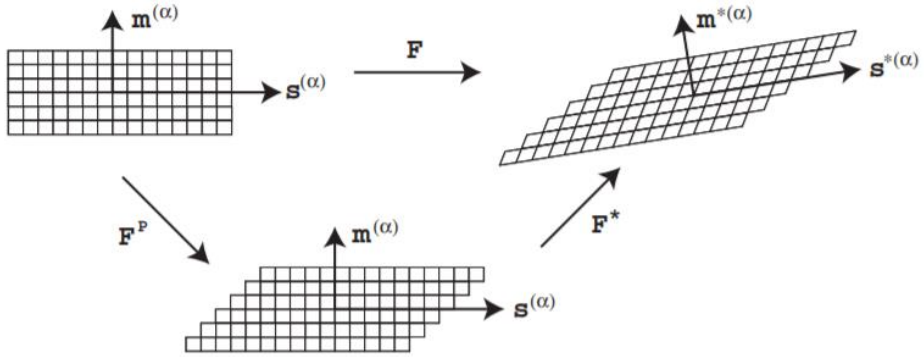

Figure 3.3 Schematic showing the final configuration of the macroscopic after combining the pure elastic and pure plastic components (Swapnil thesis [2009])

3.2.2 Constitutive Modeling

Before discussing the constitutive formalism in the context of this work, it is worth mentioning the background of the stress rate and why we need our constitutive law in the rate form and not in the simple Hookean form.

In continuum mechanics, stress rates are time derivatives of the stress that do not depend on the frame of reference. Many constitutive equations are designed in the form of a relation between a stress-rate and a strain-rate also knows as rate of deformation tensor. The mechanical response of a material should not depend on the frame of reference. In other words, material constitutive equations should be frame-indifferent which is also called the objectivity of stress tensor. If the stress and strain measures are material quantities, then objectivity is automatically satisfied. However, if the quantities are spatial, then the objectivity of the stress-rate is not guaranteed even if the strain-rate is objective.

Some of the widely used objective stress rates are:

1. Truesdell rate of the Cauchy stress tensor,
2. Green–Naghdi rate of the Cauchy stress, and
3. Zaremba-Jaumann rate of the Cauchy stress.

Here in our work we will focus on the third variant of the stress rate so we will now derive the expression for Jaumann rate of the Cauchy stress as follows:

Starting with the most general form of linearized material form. i.e., $\sigma^{PK2} = C:E$. The 2nd Piola-Kirchhoff stress and Green strain tensors are paired together because of their compatibility, i.e., both are defined in the reference configuration. The next step is to substitute the transformation from Cauchy stress to 2nd Piola-Kirchhoff stress. This gives

$$JF^{-1}.\sigma.F^{-T} = C:E \qquad \ldots(3.11)$$

Solving for the Cauchy Stress we obtain

$$\sigma = \frac{1}{J}F.(C:E).F^{T} \qquad \ldots(3.12)$$

Now we take the time derivative to obtain as follows

$$\dot{\sigma} = -\left(\frac{\dot{J}}{J^2}\right)F.(C:E).F^{T} + \frac{1}{J}\dot{F}.(C:E).F^{T} + \frac{1}{J}F.\left(C:\dot{E}\right).F^{T} + \frac{1}{J}F.(C:E).F^{\cdot T} \qquad \ldots(3.13)$$

Now Substitute the quantities in various forms in the above equation we get as

$$tr(D) = \frac{\dot{J}}{J} \quad , \quad \dot{F} = L.F \ , \quad F^{\cdot T} = F^{T}.L^{T} \quad \& \quad \dot{E} = F^{T}.D.F \qquad \ldots(3.14)$$

And then after substituting the above we later substitute $\sigma = \frac{1}{J}F.(C:E).F^{T}$

Now writing the simplified expression as follows:

$$\dot{\sigma} = -tr(D)\sigma + L.\sigma + \sigma.L^{T} + \left(\frac{1}{J}\right)F.\left(C:(F^{T}.D.F)\right).F^{T} \qquad \ldots(3.15)$$

$$\dot{\sigma} - L.\sigma - \sigma.L^{T} = -tr(D)\sigma + \left(\frac{1}{J}\right)F.\left(C:(F^{T}.D.F)\right).F^{T} \qquad \ldots(3.16)$$

The term $tr(D)$ is negligible in most of the cases. In, fact it is identically zero in incompressible materials. The term containing C represents rigid body rotation. The left hand side is called as the Lie derivative of the Cauchy Stress and hence the complete expression is in contracted form

is written in the next equation. So, we now come up with the constitutive modelling framework given by Hill and Rice.

Following the works of Hill and Rice (1972), the existence of an elastic potential $\phi = \phi(F^*)$, assures that the relation between the symmetric rate of stretching of the lattice, D*, and $\dot{\sigma}$ the Jaumann rate of Cauchy stress σ ,is given by

$$\sigma^{\nabla^*} + \sigma(I : D^*) = L : D^* \qquad \ldots(3.17)$$

where I is the second order identical tensor, L is the tensor of elastic moduli having the full set of symmetries $L_{ijkl} = L_{jikl} = L_{ijlk} = L_{jilk}$, the Jaumann rate σ^{∇^*} is the corotational stress rate on axes that rotate with the crystal lattice, which is related to the corotational stress rate on axes rotating with the material, σ^{∇}, by

$$\sigma^{\nabla^*} = \sigma^{\nabla} + (\Omega - \Omega^*).\sigma - \sigma.(\Omega - \Omega^*) \qquad \ldots(3.18)$$

$$, where \quad \sigma^{\nabla} = \dot{\sigma} - \Omega.\sigma + \sigma.\Omega$$

The crystalline slip is assumed here to obey Schmid's law, i.e. the slipping rate $\dot{\gamma}^{\alpha}$in any particular slip system α is assumed to depend on the current σ solely through the so-called Schmid stress,τ^{α}. The Schmid stress is just the resolved shear stress when elastic lattice distortions are negligible. There are many possible generalizations in the presence of finite elastic distortions, some discussed by Asaro and Rice (1977). Here we use the version based on the Rice's (1971) thermodynamic stress conjugate to slip, which Rice has shown to precisely preserve the normality structure of the small deformation theory (Mandel, 1965; Hill, 1967; Rice, 1970) in terms of work conjugate stress and strain measures for finite deformation. Thus we use the definition:

$$\tau^{\alpha} = m^{*\alpha}.\ (\frac{\rho_0}{\rho})\sigma.\ s^{*\alpha} \qquad \ldots.(3.19)$$

where ρ_0 and ρ are the mass density in the reference and current states; Hill and Rice (1972) note that this τ^{α}; τ_s^m the mixed shear component of Kirchhoff stress τ on coordinates which convect with the lattice. The rate of change of this Schmid stress is given by:

$$\dot{\tau}^{\alpha} = m^{*\alpha}.\left[\sigma^{\nabla^*} - D^*.\sigma + \sigma.D^*\right].s^{*\alpha} \qquad \ldots(3.20)$$

For our work, we need a model which can capture the effect of wide range of strain rate and also captures the orientation effect as well at the same time which is more physics based and relates to the fundamental aspects of slip mechanism . Hence, we chosen the model formalism given by Khan et al. [2015] . So in the next section we will discuss the various aspects of the dislocation density based model and also the background of certain forms of the equations as opposed to directly digesting it , we will investigate critically to the forthcoming equations.

3.3 Dislocation-density based physical model

A single crystal plasticity model based on dislocation densities is used in this work based on the model developed by Khan et al.[2015] in which they consider that the slipping and hardening of each slip system are the results of dislocation movement, evolution and interaction. The framework and kinematic of the classical model still hold with now a new flow rule and a hardening law that are based on dislocation densities. In addition, an evolution model of dislocation densities with deformation was added.

The strengths of slip systems are assumed to be functions of the dislocation densities. A athermal strength g_{ath} and a thermal strength g_{th} are assigned for each and every slip system .Thermal strengths represent the short-range resistances that are due to short-range obstacles (~10 atomic diameters) such as lattice friction (Peierls–Nabarro stress), solute atoms and forest dislocations. Short-range resistances can be overcome at a lower applied shear stress with the help of thermal activation. The corresponding equation of the thermal strength is represented by equation (3.22). At the same time, the athermal strengths are the long-range resistances that cannot be overcome with the help of thermal activation, which are due to long-range obstacles such as large incoherent precipitates and long-range interaction with other dislocations. With the help of the schematic we can also understand the short- and long-range resistances build by the activities of the dislocations within a grain as shown in the Figure 3.4. As discussed in the introduction, dislocation glide is still considered to be the most important deformation mechanism of FCC materials. However, due to the very small grain size, there will be almost no dislocation interactions within the grain. Now dislocation lines nucleate from the GB (Grain boundary) on one side of the grain, unpin from GB obstacles, propagate through the entire grain and get absorbed or accumulated at the GB on the other side of the grain. Usually the short-range resistances are ignored being negligibly small and Dislocations require a larger resolved shear stress to propagate than to nucleate. An externally applied

resolved shear stress, ta on the slip system a, is needed to further move the dislocation forward. However, the net driving force of dislocation movement is the effective shear stress: $\tau_{eff} = \tau^{\alpha} - \tau_{ath}$ .And there is a pinning of dislocations with the grain ledges and in turn the effective stress bow the dislocation and then the net effective force in the direction of dislocation movement is given by F .

$$g_{th}^{\alpha} = \mu b \sqrt{\sum_{\beta} A_{\alpha\beta} \rho^{\beta}} \quad \text{….(3.22a)}$$

$$g_{ath}^{\alpha} = \mu b \sqrt{\sum_{\beta} B_{\alpha\beta} \rho^{\beta}} + \frac{k_0}{d^{n_*}} \quad . \quad \text{….(3.22b)}$$

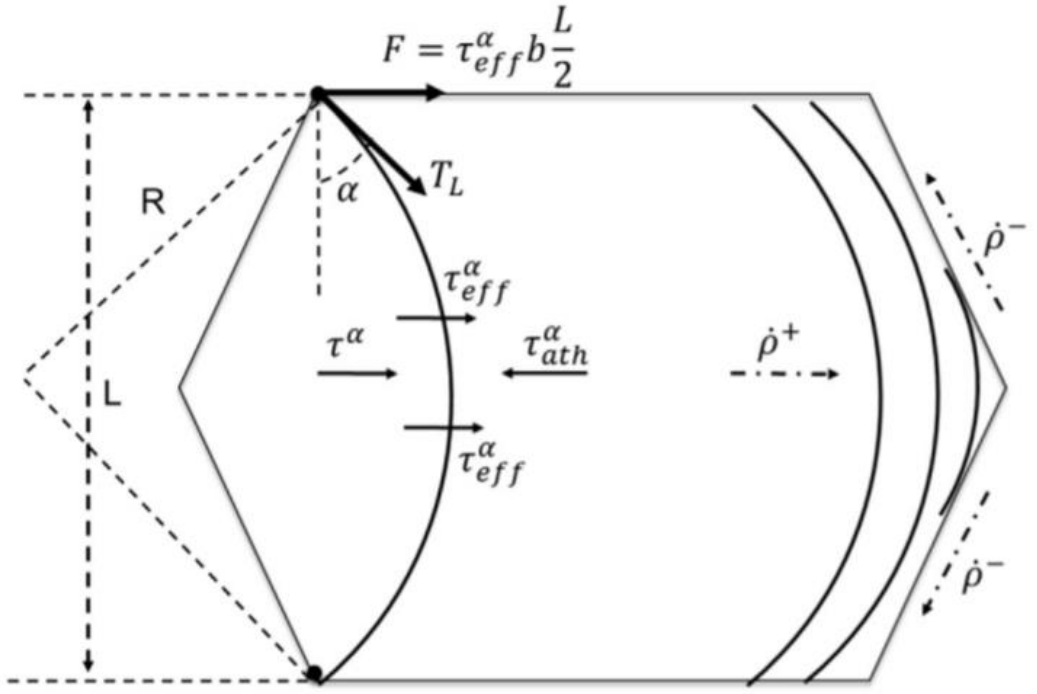

Figure 3.4 Schematic showing how the long range resistances are countered by the applied resolved stress and then how it influences the dislocation density (in this case increase) within a grain (Liu et al.[2016])

After the propagation through the entire grain, the dislocations reach the GB on the other side of the grain. The dislocations need to be "absorbed" by the GB otherwise they would pile-up in front of the GB and cause the internal stress $\tau_{ath,\rho}$. Therefore, at the absorption side of the grain, there is a competition between the incoming and the absorption of dislocations.

The increase (or not) of dislocation density is the result of such a competition. The net accumulation rate of dislocations $\dot{\rho}_\alpha$ is determined by the generation rate $\dot{\rho}_{\alpha+}$ and the absorption rate $\dot{\rho}_{\alpha-}$. The generation of dislocations is simple and straightforward. When a dislocation line traverses the entire grain, it would produce a plastic shear strain of γ =b/d. It also corresponds to the generation of a dislocation length of d at the GB (increase of dislocation density is $1/d^2$). Hence, the generation rate of dislocation density is:

$$\dot{\rho}_{\alpha+} = \left(\frac{1}{d^2}\right)\left(\frac{d}{b}\right)\dot{\gamma}^\alpha = \left(\frac{1}{bd}\right)\dot{\gamma}^\alpha \quad \ldots(3.23)$$

The absorption process of dislocations by GB is more complicated. The free volume brought by the incoming dislocations should be accommodated be the shuffling of atoms, most probably by diffusion along the boundary (Bouaziz et al., 2010). So, the recovery rate should be proportional to the diffusivity at the GB, which could be assumed to be grain-size independent but depends on the temperature and other variables related to the GB properties. If there is already a pile-up of dislocations, the absorption is favored by the elastic field at the head of the pile-up. So, the higher the dislocation density, the faster the absorption rate. Taking into account the two aforementioned considerations, we propose the absorption rate of dislocations at GB as:

$$\dot{\rho}_{\alpha-} = \frac{y_c\dot{\gamma}^\alpha}{b} = y_0 \exp\left(-\triangle\frac{G_{GB}}{KT}\right)\rho\dot{\gamma}^\alpha \quad \ldots(3.24)$$

Hence the net accumulation rate of the dislocation can we written after simplifying and changing some symbol viz, d to K etc. as:

$$\dot{\rho}^\alpha = (1/b)\left(\frac{\sqrt{\sum_\beta C_{\alpha\beta}\rho^\beta}}{K} - 2y_c\sum_\beta D_{\alpha\beta}\rho^\beta\right)\dot{\gamma}^\alpha \quad \ldots(3.25)$$

With such a localized force F = $\frac{\tau^\alpha_{eff}bL}{2}$ on the GB obstacle in the direction of dislocation movement, the dislocation can overcome (unpin) this obstacle. The total energy needed to overcome the obstacle is the total activation energy$\triangle G_0$, which can be represented by the total area under the force-distance curve (Fig. 3.5). At 0 K, this energy barrier needs to be overcome purely by mechanical force since there is no thermal activation. Hence, a maximum force $Fmax$ is needed at 0 K which can be related to $\triangle G_0$ by:

$$\triangle G_0 = Fmax * w_0 \quad \ldots(3.26)$$

where w_0 as the average travel distance of the dislocation in the overcoming process.

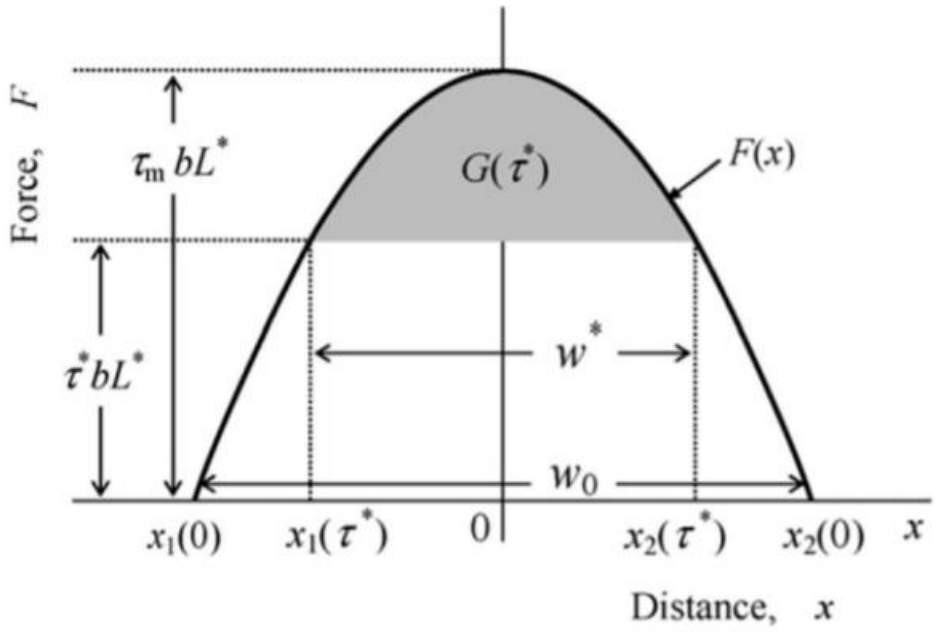

Figure 3.5 Schematic showing the force-distance diagram of the short-range GB obstacle (Kato, 2009). The x axis represents the position of the dislocation with respect to the obstacle while the F axis represents the force needed to maintain the dislocation at a certain position x (without thermal fluctuations, i.e., at 0 K).

Now we can define thermal strength τ_{th} as the maximum effective shear stress corresponding to Fmax, to mechanically overcome the obstacle at 0 K.

$$\frac{\triangle G_0}{w_0} = Fmax = \frac{\tau_{th}^{\alpha} bL}{2} \quad \ldots.(3.27)$$

At 0 K, the effective shear stress τ_{eff}^{α} needs to be equal to the thermal strength τ_{th}^{α} for the dislocation to overcome the obstacle purely by mechanical force. At a temperature larger than 0 K, the needed τ_{eff}^{α}should be larger than zero but can be smaller than the thermal strength τ_{th}^{α}) since there is help from thermal activation in addition to mechanical force. The energy barrier is lowered by the work done by $\tau_{eff}^{\alpha}$and the reduced activation energy $\triangle G$ will be overcome by

the thermal activation. The reduced activation energy $\triangle G$ can be approximated by a phenomenological form (Caillard and Martin, 2003):

$$\triangle G = \triangle G_0 \left(1 - \left(\frac{\tau_{eff}^{\alpha}}{\tau_{th}^{\alpha}}\right)^{p}\right)^{q} \quad \ldots (3.28)$$

where p, q are the parameters related to the profile of the force-distance diagram (shape of the curve in Fig. 2). The frequency v of successfully overcoming the obstacle can be related to the activation energy via an Arrhenius-type equation:

$$v = v_0 \exp\left(-\triangle \frac{G}{kT}\right) \quad \ldots(3.29)$$

Here, v_0 is the attempt frequency and KT represents the energy from thermal activation which is the product of Boltzmann constant K and temperature T (Caillard and Martin, 2003). Using all the equations results in the following flow rule:

$$\dot{\gamma}^{\alpha} = \begin{cases} 0 & , |\tau^{\alpha}| \leq g^{\alpha} \\ \dot{\gamma}_0 \exp\left\{-(\Delta F/KT)\left[1 - \left(\frac{\tau^{\alpha}}{g^{\alpha}} - 1\right)^{p}\right]^{q}\right\} & , |\tau^{\alpha}| > g^{\alpha} \end{cases} \quad \ldots.(3.30)$$

3.4 Rate tangent formulation

The tangent modulus method for rate dependent solid developed by Peirce et al. (1984) is used in the subroutine. We define the increment of shear strain $\triangle\gamma^{\alpha}$in slip system a within the time increment $\triangle$t by:

$$\Delta\gamma^{\alpha} = \gamma^{\alpha}(t + \Delta t) - \gamma^{\alpha}(t) \quad \ldots.(3.31)$$

Then we employ a linear interpolation as:

$$\Delta\gamma^{\alpha} = [\theta\dot{\gamma}\alpha(t + \Delta t)\cdot + (1 - \theta)\dot{\gamma}\alpha(t)]\Delta t\cdot \quad \ldots.(3.32)$$

The parameter θ ranges from 0 to 1, with θ =0 corresponding to the simple Euler time integration scheme. A choice of θ between 0.5 and 1 is recommended (Peirce et al. [1984]).

The slipping rate in general is a function of the resolved shear stress and the current strength as follows:

$$\dot{\gamma}^{\alpha} = \dot{\gamma}^{\alpha}(\tau^{\alpha}, g^{\alpha}, T) \quad \text{....(3.33)}$$

Since we are using the linear interpolation, we will do the Taylor's expansion of the slipping rate taking into account only the linear terms as follows:

$$\dot{\gamma}^{\alpha}(t + \Delta t) = \dot{\gamma}^{\alpha}(t) + \frac{\partial \dot{\gamma}^{\alpha}}{\partial \tau \alpha}\Big| \Delta\tau^{\alpha} + \frac{\partial \dot{\gamma}^{\alpha}}{\partial T}\Big| \Delta T + \frac{\partial \dot{\gamma}^{\alpha}}{\partial g^{\alpha}}\Big| \Delta \mathrm{g}^{\alpha} \quad \text{....(3.34)}$$

where $\Delta\tau^{\alpha}$ and $\Delta \mathrm{g}^{\alpha}$ are the increments of resolved shear stress and current strength in Slip system a within the time increment Δt, respectively. Now rearranging the above equations to get the following incremental relation:

$$\Delta\gamma^{\alpha} = \Delta t \left[\dot{\gamma}^{\alpha}(t) + \theta \left(\frac{\partial \dot{\gamma}^{\alpha}}{\partial \tau^{\alpha}}\right) \Delta\tau^{\alpha} + \theta \left(\frac{\partial \dot{\gamma}^{\alpha}}{\partial g^{\alpha}}\right) \Delta g^{\alpha} \right] \quad \text{....(3.35)}$$

Recalling, $\mu_{ij}^{\alpha} = 1/2\left(s_i^{*\alpha} m_j^{*\alpha} + s_j^{*\alpha} m_i^{*\alpha}\right)$; $\omega_{ij}^{\alpha} = 1/2\left(s_i^{*\alpha} m_j^{*\alpha} - s_j^{*\alpha} m_i^{*\alpha}\right)$ & $\Omega_{ij} - \Omega_{ij}^{*} = \sum_{\alpha} \omega_{ij}^{\alpha} \dot{\gamma}^{\alpha}$ and now taking the increment of the strength equation we have,

$\Delta g^{\alpha} = \sum_{\beta} h_{\alpha\beta} \Delta\gamma^{\beta}$ where $h_{\alpha\beta}$ will be derived in terms of dislocation density in the subsequent sections.

So now taking the increment form of the resolved shear stress using the constitutive formalism and thereafter taking the increment of the stress using the Schmid's law we obtain:

$$\Delta\tau^{\alpha} = [L_{ijkl}\mu_{kl}^{\alpha} + \omega_{ik}^{\alpha}\sigma_{jk} + \omega_{jk}^{\alpha}\sigma_{ik}].[\Delta\epsilon_{ij} - \sum_{\beta} \mu_{ij}^{\beta} \Delta\gamma^{\beta}] \quad \text{....(3.36)}$$

$$\Delta\sigma_{ij} = L_{ijkl}\Delta\epsilon_{kl} - \sum_{\alpha}[L_{ijkl}\mu_{kl}^{\alpha} + \omega_{ik}^{\alpha}\sigma_{jk} + \omega_{jk}^{\alpha}\sigma_{ik}]\Delta\gamma^{\alpha} \quad \text{....(3.37)}$$

For given strain increments $\Delta\epsilon_{ij}$ the increments of shear strain $\Delta\gamma^{\beta}$ in the slip systems are uniquely determined by the following linear algebraic equation, which is obtained by substituting the above incremental form of the resolved shear stress , stress and the internal resistance in the resulting incremental formulation , we obtain:

$$\sum_\beta \left\{\delta_{\alpha\beta} + \theta\Delta t \left(\frac{\partial\dot{\gamma}^\alpha}{\partial\tau^\alpha}\right)[L_{ijkl}\mu_{kl}^\alpha + \omega_{ik}^\alpha\sigma_{jk} + \omega_{jk}^\alpha\sigma_{ik}]\mu_{ij}^\beta - \right.$$
$$\left. \theta\Delta t \left(\frac{\partial\dot{\gamma}^\alpha}{\partial g^\alpha}\right) H_{\alpha\beta} sign(\dot{\gamma}_t^\beta) \right\} \Delta\gamma^\beta \quad = \dot{\gamma}_t^\alpha \Delta t + \theta\Delta t(\partial\dot{\gamma}^\alpha/\partial\tau^\alpha)[L_{ijkl}\mu_{kl}^\alpha + \omega_{ik}^\alpha\sigma_{jk} + \omega_{jk}^\alpha\sigma_{ik}]\Delta\epsilon_{ij}$$

….(3.38)

Note, this definition of stress increment is consistent with the Finite element code ABAQUS (ABAQUS theory manual, 1989; also Hughes and Winget, 1980) for Finite deformation analysis.

Now we will consider the effects of lattice rotation since we know that the material while deforming undergo rigid body rotation and so the rotation effect should not come in the formulation of stress rate i.e., Objectivity of stress should be preserved . The crystal lattice undergoes distortion and rotation as the crystal deforms ; however, the effect of lattice rotation does not explicitly appear in the constitutive equations in Section 2 when all rate quantities are formed on this rotating lattice frame (Asaro and Rice [1977]) .

The lattice deformation and rotation are fully characterized by the reciprocal vectors coinciding with slip directions, s*(a), and normal to slip planes, m*(a), in the deformed configuration. Now we will differentiate the equations for slip system vectors to obtain as:

$$\dot{s}^{*\alpha} = L^*.s^{*\alpha} \quad \text{….(3.39)}$$

And $\dot{m}^{*\alpha} = -m^{*\alpha}.L^*$ ….(3.40)

Now the corresponding incremental formulation of the above equation is written as follows:

$$\Delta s_i^{*\alpha} = \left\{\Delta\epsilon_{ij} + \Omega_{ij}\Delta t - \sum_\beta[\mu_{ij}^\beta + \omega_{ij}^\beta]\Delta\gamma^\beta\right\}s_j^{*\alpha} \quad \text{….(3.41)}$$

And $\Delta m_i^{*\alpha} = -m_j^{*\alpha}\left\{\Delta\epsilon_{ij} + \Omega_{ij}\Delta t - \sum_\beta[\mu_{ij}^\beta + \omega_{ij}^\beta]\Delta\gamma^\beta\right\}$ ….(3.42)

The s*(a) and m*(a) are updated at each time step so as to obtain the "Schmid factor" μ_{ij}^β and the rotation tensor ω_{ij}^β) at the current state.

Now, the general form of the hardening rule can be represented as the linear forms for the slip rates on all systems:

$$\dot{g}^{\alpha} = \sum_{\beta=1}^{12} h_{\alpha\beta}\dot{\gamma}^{\beta} \quad \text{….(3.43)}$$

Now taking the derivative of strength equation in the model to obtain in rate form by taking it derivative w.r.t. time to obtain:

$$\dot{g}^{\alpha} = \mu A_{\alpha\beta}[\sqrt{\sum_{\beta=1}^{12}\rho^{\beta}}\,\frac{1}{K} - 2y_c\rho^{\beta}]\,\frac{Q}{2\sqrt{\sum_{\beta=1}^{12}A_{\alpha\beta}\rho^{\beta}}}\,\dot{\gamma}^{\beta} \quad \text{….(3.44)}$$

By comparing with the above generalized form of Taylor's kind equation we will obtain the hardening moduli for calculation of self as well as latent hardening in the slip systems. So, the hardening moduli is given as:

Hardening modulii:

$$h_{\alpha\beta} = \mu A_{\alpha\beta}[\sqrt{\sum_{\beta=1}^{12}\rho^{\beta}}\,\frac{1}{K} - 2y_c\rho^{\beta}]\,\frac{Q}{2\sqrt{\sum_{\beta=1}^{12}A_{\alpha\beta}\rho^{\beta}}} \quad \text{….(3.45)}$$

Now, since the hardening moduli as derived above is a function of dislocation density and dislocation density evolves w.r.t. to rate of deformation .Thus ,in every iteration after start its change has to be added in the above hardening moduli expression .Now ,we calculates the change in the hardening moduli as follows:

$$\frac{dh_{\alpha\beta}}{d\gamma^{\beta}} = \{-\mu A_{\alpha\beta}^{2}(\sqrt{\sum_{\beta=1}^{12}\rho^{\beta}}\,\frac{1}{K} - 2y_c\rho^{\beta})\,\frac{1}{4\left(\sqrt{\sum_{\beta=1}^{12}A_{\alpha\beta}\rho^{\beta}}\right)^{3}} + \mu A_{\alpha\beta}(\frac{1}{2K\sqrt{\sum_{\beta=1}^{12}\rho^{\beta}}} - 2y_c)\}\frac{d\rho^{\beta}}{d\gamma^{\beta}}$$

….(3.46)

$$\text{Where, } \frac{d\rho^{\beta}}{d\gamma^{\beta}} = (\sqrt{\sum_{\beta=1}^{12}\rho^{\beta}}\,\frac{1}{bK} - \frac{2}{b}y_c\rho^{\beta}) \quad \text{….(3.47)}$$

Now here $A_{\alpha\beta}$ is an interaction matrix with 6 independent constants. It is worthwhile to look into this matrix and understand the physical significance of these constants. Table 3.1 (Franciosi and zaoui [1981]) presents the rationale for assigning values to the amplitude factors, taking all

possible dislocation interactions into account. For instance, coplanar interactions tend to be weaker compared to their anti–planar counterparts and thus the associated amplitude factors must take this into account.

FCC single crystals display five different interaction types, leading to the definition of 6 independent $A_{\alpha\beta}$ components. These distinct slip interactions between systems α and β are subject to the type of dislocation junction formed, which consequently translates into the relative orientation of the systems. This classification of interactions results into the definition of the five distinct constants αi (where i = 1, 2, . . . , 5) as follows:

	A2	A3	A6	B2	B4	B5	C1	C3	C5	D1	D4	D6
A2	SH^{a^0}	$Copl^{a^1}$	$Copl^{a^1}$	CS^{a^1}	GJ^{a^2}	GJ^{a^2}	HL^{a^1}	GJ^{a^2}	LC^{a^3}	HL^{a^1}	LC^{a^3}	GJ^{a^2}
A3	$Copl^{a^1}$	SH^{a^0}	$Copl^{a^1}$	GJ^{a^2}	HL^{a^1}	LC^{a^3}	GJ^{a^2}	CS^{a^1}	GJ^{a^2}	LC^{a^3}	HL^{a^1}	GJ^{a^2}
A6	$Copl^{a^1}$	$Copl^{a^1}$	SH	GJ	LC	HL^{a^1}	LC^{a^3}	GJ^{a^2}	HL^{a^1}	GJ^{a^2}	GJ^{a^2}	CS^{a^1}
B2				SH	Copl	Copl	HL	LC	GJ	HL	GJ	LC
B4					SH	Copl	LC	HL	GJ	GJ	CS	GJ
B5						SH	GJ	GJ	CS	LC	GJ	HL
C1							SH	Copl	Copl	CS	GJ	GJ
C3								SH	Copl	GJ	HL	LC
C5									SH	GJ	LC	HL
D1										SH	Copl	Copl
D4											SH	Copl
D6												SH

Table 3.1: Strength amplitude factors $A_{\alpha\beta}$ defining the intensity of cross–hardening interactions on FCC crystals.

SH : Self hardening (a_0)

Copl: Coplanar syst. (a_1).

CS: Colinear syst. (cross slip) (a_2).

HL: Hirth Lock syst. pair with normal slip directions (a_4).

GJ: Systems pair leading to Glissile junctions formation (a_3).

LC: Systems pair leading to Lomer-Cottrelt sessile locks formation (a_5)

The symbolic notation of various other symbols used in the table 3.1 is represented in the subsequent tables .

Notation	**Slip plane**
A	**($\bar{1}$ 1 1)**
B	**(1 1 1)**
C	**($\bar{1}$ $\bar{1}$ 1)**
D6	**(1 $\bar{1}$ 1)**

Table 3.2 Notations for Slip Planes (Refer Franciosi and zaoui[1982])

Notation	**Slip direction**
1	[0 1 1]
2	[0 $\bar{1}$ 1]
3	[1 0 1]
4	[$\bar{1}$ 0 1]
5	[$\bar{1}$ 1 0]
6	[1 1 0]

Table 3.3 Notations for Slip Directions (Refer Franciosi and zaoui[1982])

Now what these various interactions are viz, the term included in the main diagonal of the hardening matrix and the term which are included in the off diagonal of the hardening matrix and their physical significance is discussed briefly as follows:

• Self Hardening: The Burgers vectors of systems α and β are unaffected by this interaction.

• (Hirth Lock): The Burgers vectors resulting from the interaction between systems α and β is not energetically admissible.

• Coplanar Junction: The Burgers vector resulting from the interaction between systems α and β is on the same plane as the original ones.

• Glissile Junction: The Burgers vector resulting from the interaction between systems α and β is energetically admissible and on one of the two slip planes.

• Sessile Junction: The Burgers vector resulting from the interaction between systems α and β is energetically admissible but not on neither of the two slip planes.

• Collinear system: The Burgers vector resulting from the interaction between slip systems α and β of the different plane such that it gives rise to cross slip.

Now we will give the sketch of the Integration algorithm developed for this work which subsequently is implemented in the UMAT.

3.5 Integration algorithm

The integration algorithm is the basis of this whole work and it taken a lot of time to formulate it by connecting all the dots of various studies available in the literature.

Given: $F_n,\ F_n^*,\ \Delta\epsilon_{n+1} = D_n\Delta t,\ \Delta t = t_{n+1} - t_n,\ \tau_n^\alpha,\ g_n^\alpha,\ \gamma_n^\alpha,\ \sigma_n^\alpha,\ m_n^\alpha,\ s_n^\alpha,\ \rho_n^\alpha$ the stress update using the above algorithm works as follows :-

Step 1: Compute $s^{*\alpha} and\, m^{*\alpha}$ in the deformed configuration using tensor transformation equation of (3.2). Also compute the Elasticity tensor in the current configuration.

Step 2: Compute using (3.7 & 3.8), the values of $\mu^\alpha\ and\ \omega^\alpha$ in the current time step.

Step 3: Compute using (3.9 & 3.10) ,the values of $D_{ij} - D_{ij}^{*}$ and $\Omega_{ij} - \Omega_{ij}^{*}$ in the current time step as

Step 4: Compute τ_n^{α} , $g_n^{\alpha}$from (3.19 & 3.22a,b) and check whether $|\tau_n^{\alpha}| \geq g^{\alpha}$,if yes go to step 5 otherwise , perform an elastic step.

Step 5: If yes, then firstly compute $\frac{d\dot{\gamma}^{\alpha}}{d\left(\frac{\tau^{\alpha}}{g^{\alpha}}\right)}|_n$from (3.27) which is the flow rule of the model and then compute $h_{\alpha\beta}{}_n$ & $dh_{\alpha\beta_n}$ using (3.45 & 3.46 & 3.47).

Step 6: Compute $\Delta\gamma_{n_{+1}}{}^{\alpha}$ using Modified Newton- rhapson iterative method / linear incremental formulation. In this study we used the latter one but the former one though complex is more computationally efficient.

Step 7: Compute $\Delta g_{n+1}^{\alpha}, \Delta\tau_{n+1}^{\alpha}$, $\Delta\sigma_{n+1}^{\alpha}$, $\Delta s^{*a}{}_{n+1}$, $\Delta m^{*a}{}_{n+1}$, $\Delta\rho_{n+1}^{\alpha}$ i.e., the increment in the next time step using incremental relations from (3.37 to 3.44) .

Step 8: Now we will update $\gamma^{\alpha}, \tau^{\alpha}, g^{\alpha}, \sigma^{\alpha}, \rho^{\alpha}, m^{*\alpha}, s^{*\alpha}$, L^{P} for the next iteration .

Step 9: Finally, we update using values obtained from above the Jacobian where the generalised expression of Jacobean $= \partial\Delta\sigma/\partial\Delta\epsilon$.

Step 10: Check $|\Delta\dot{\gamma}_{n+1}^{\alpha}| > \gamma_{err}^{\alpha}$(tolerance) to see whether the solution i.e., the value of shear strain obtained in the current step gets converged or not .

Step 11: If no, then we will again the procedure from step 5 onwards. Otherwise, we will save the solutions and will stop the algorithm.

In the next page Figure 3.6 shows the integration algorithm in the tabular form.

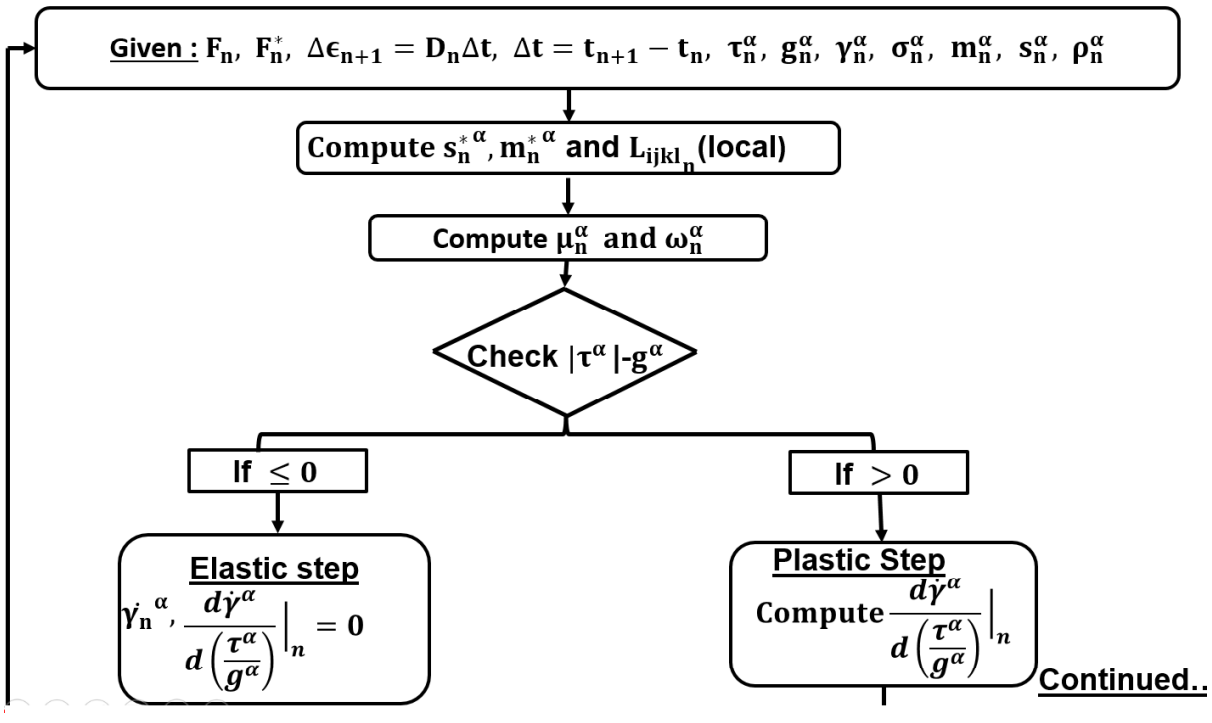
Given : $F_n,\ F_n^*,\ \Delta\epsilon_{n+1} = D_n\Delta t,\ \Delta t = t_{n+1} - t_n,\ \tau_n^\alpha,\ g_n^\alpha,\ \gamma_n^\alpha,\ \sigma_n^\alpha,\ m_n^\alpha,\ s_n^\alpha,\ \rho_n^\alpha$
Compute $s_n^{*\alpha}, m_n^{*\alpha}$ and L_{ijkl_n}(local)
Compute μ_n^α and ω_n^α
Check $|\tau^\alpha|$-g^α
If ≤ 0
If > 0
Elastic step
$\dot{\gamma}_n^\alpha, \frac{d\dot{\gamma}^\alpha}{d\left(\frac{\tau^\alpha}{g^\alpha}\right)}\Big|_n = 0$
Plastic Step
Compute $\frac{d\dot{\gamma}^\alpha}{d\left(\frac{\tau^\alpha}{g^\alpha}\right)}\Big|_n$
Continued..

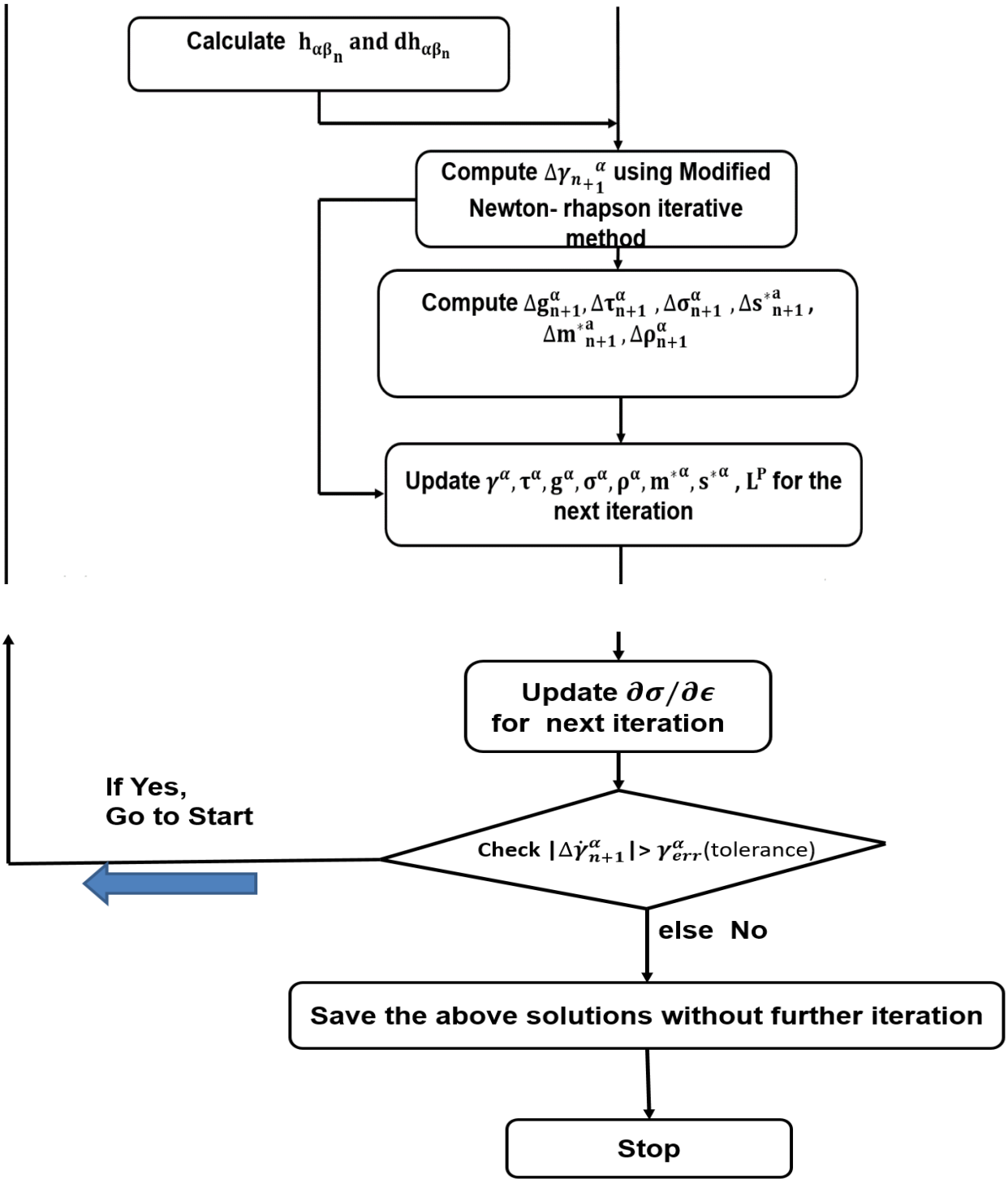

Figure 3.6: The Integration algorithm based on the hardening law relying on the dislocation density and the flow based on the physics of thermal activation .

3.6 Simulation and discussion

In the current section, we present the results from the finite element simulations on single crystal specimens subjected to a series of uniaxial tension experiments. All finite element analyses were performed using the Abaqus general purpose finite element software and the rate independent crystal plasticity model was computationally implemented in the form of a UMAT (User Material) subroutine. The UMAT subroutine uses the rate tangent algorithm (see Section above) to iteratively predict the set of active systems and perform the numerical integration of the constitutive equations. All uniaxial tension simulations were performed using the Static/General step option within the Abaqus/Standard module of the Abaqus software.

3.6.1 Flow rule parameters:

$\dot{\gamma}_0(s^{-1})$	⍙F	P	q
1.732e6	3e-19	0.141	1.1

3.6.2 Hardening law parameters:

a_0	a_1	a_2	a_3	a_4	a_5
0.08	**0.22**	**0.30**	**0.38**	**0.16**	**0.45**

3.6.3 Dislocation evolution parameters

ρ_0^α	K	y_c
1e9	**38**	**3.56**

Table 3.4 Input Parameters used for the simulation of aluminum single crystal .

Parameters of the flow rule were adopted from *Balasubramanian and Anand (2002),* which were obtained by fitting against the experimental data of 99% percent pure polycrystal aluminum by *Carreker and Hibbard (1957).*

Parameters for the thermal and athermal strength are two interaction matrices A_{ab} *and* B_{ab} comes *from Franciosi and zaoui (1982) and Arsenlis and Parks (2002).*

Refer: *Cottrell and Stokes (1955), Balasubramanian and Anand (2002)* we obtained $\{A_{ab}\}/\{B_{ab}\} = 1$ and micro hall − petch term is ignored in our model too.

3.7 One Element Test of a Single FCC Aluminium Crystal

The simulation on Aluminium single crystal single element is carried out in two kinds of orientations. One is S1 kind and the other is S2 type. Orientation S1 is well within the standard stereographic triangle, therefore a single slip mode is expected. Although to be more accurate, in the rate-dependent (visco-plastic) theory, there will always be small amount of shear strain rate on every slip system since usually there will always be some amount of resolved shear stress on every slip system. However, with a loading direction well within the standard triangle such as S1, the shear strain rate on slip systems other the primary one is negligible.

S2 is close to the 110 direction with a small mis-orientation, so multi-slip is possible according to the rate-dependent approach. In rate-dependent approach, depending on the model parameters (such as the strain rate sensitivity index m in the power-law flow rule), it is possible that slip systems other than the primary one have significant amounts of shear strain rate when the S2 is close to 110 direction.

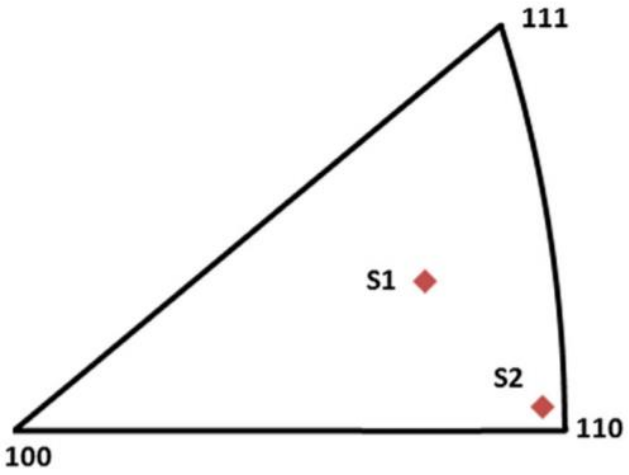

Figure 3.6 The orientations S1 and S2 in a standard stereographic triangle .

A general purpose C3D8R (reduced integration) element is used in this work with some hourglass stiffness which will be required since at high strain rate the single element will get twist and distort if we did not put the hourglass stiffness . Tensile load is applied in one of the face nodes of the elements and the other face will be restricted by applying roller support opposite to the tensile direction and also to restrict rigid body motion we applies roller support of the second and the third direction in the opposite face nodes . Also , we will control the strain rate of different magnitudes using the input file .

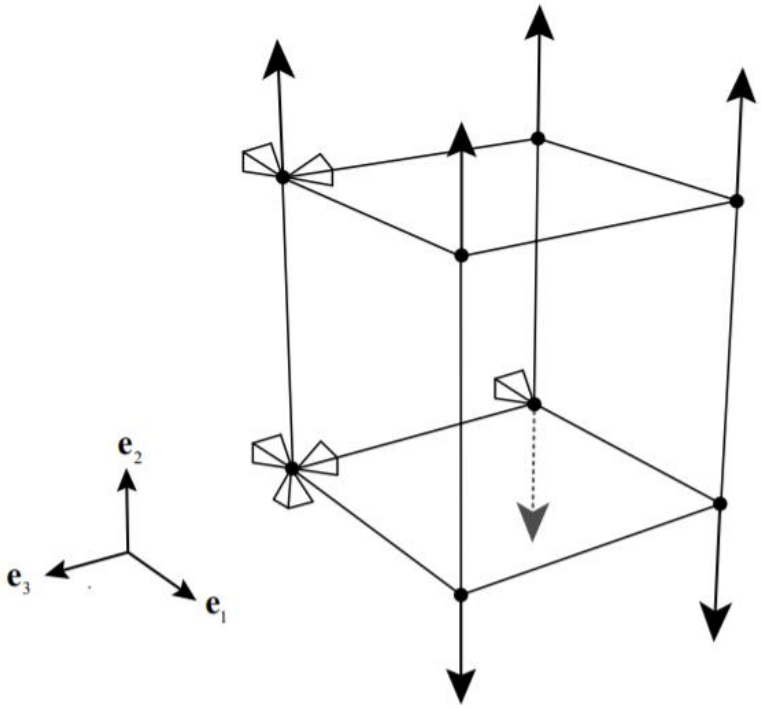

Figure 3.6 (b); Schematic illustration of the prescribed boundary conditions and the force field (tension) applied to the single element single crystal Aluminium. It can be mathematically proven that a minimum of 6 displacement d.o.f. need to be constrained to eliminate rigid body motions and rotations in 3D analyses.

3.8 Results and Discussions

The stress strain curve for multi slip corresponding to the high rate of deformation is presented in the Figure 3.7. The simulation curve has an initial bump corresponding to the elastic limit & it shows little deviation from the experimental curve in the initial part of stretching and then it starts to converge with the experimental plot. The curves produced by Khan et al. [2015] has similar deviation to the experimental but in the opposite direction.

In all, the simulation curve of this study slightly overly estimates the hardening /hardening rate.

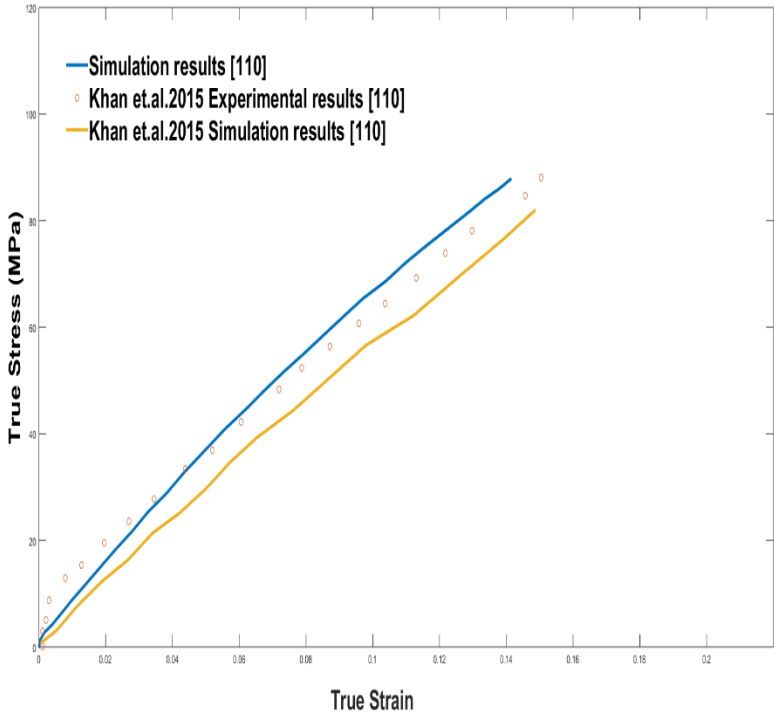

Fig. 3.7: Stress-Strain curves of single crystal with orientation S2 at a strain rate of 1000/s

The stress strain curve for multi slip corresponding to the initial part of high rate regime is presented in the Figure 3.8. The simulation curve has an initial bump corresponding to the elastic limit & it shows little deviation from the experimental curve in the initial part of stretching and then it converges with the experimental plot. The curves produced by Khan et al. [2015] deviation to the experimental goes till the full stretch.

In all, the simulation curve of this study matches well with the experimental plot.

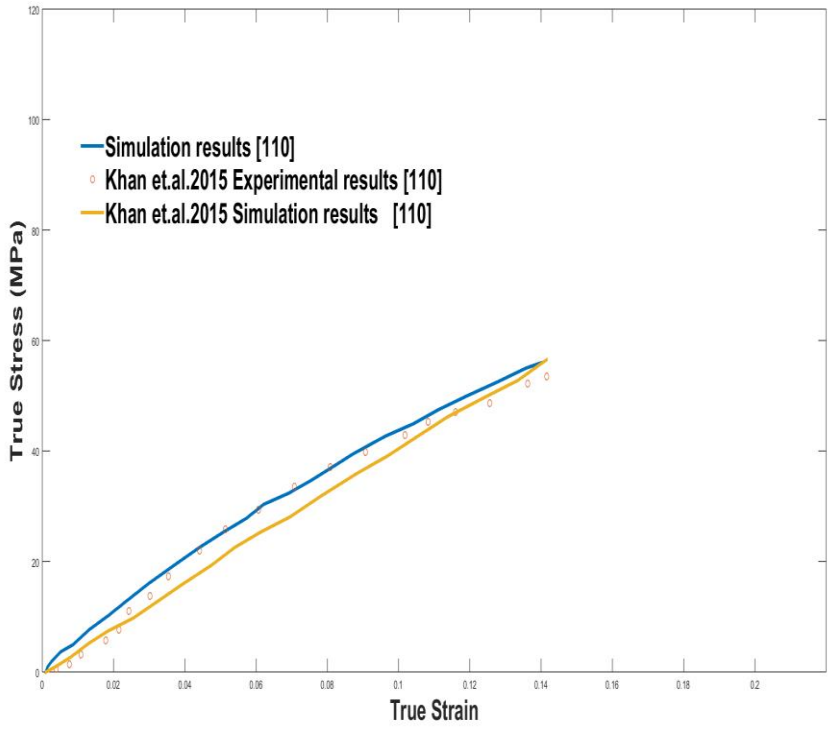

Fig.3.8: Stress-Strain curves of single crystal with orientation S2 at a strain rate of 0.001/s

The stress strain curve for single slip corresponding to the high rate of deformation is presented in the Figure 3.9. The simulation curve has an initial bump corresponding to the elastic limit & it shows some significant deviation from the experimental curve in the initial part of stretching and then it starts to converge with the experimental plot. The curves produced by Khan et al. [2015] has similar deviation to the experimental in the same direction as well.

In all, the simulation curve of this study underestimate the hardening /hardening rate.

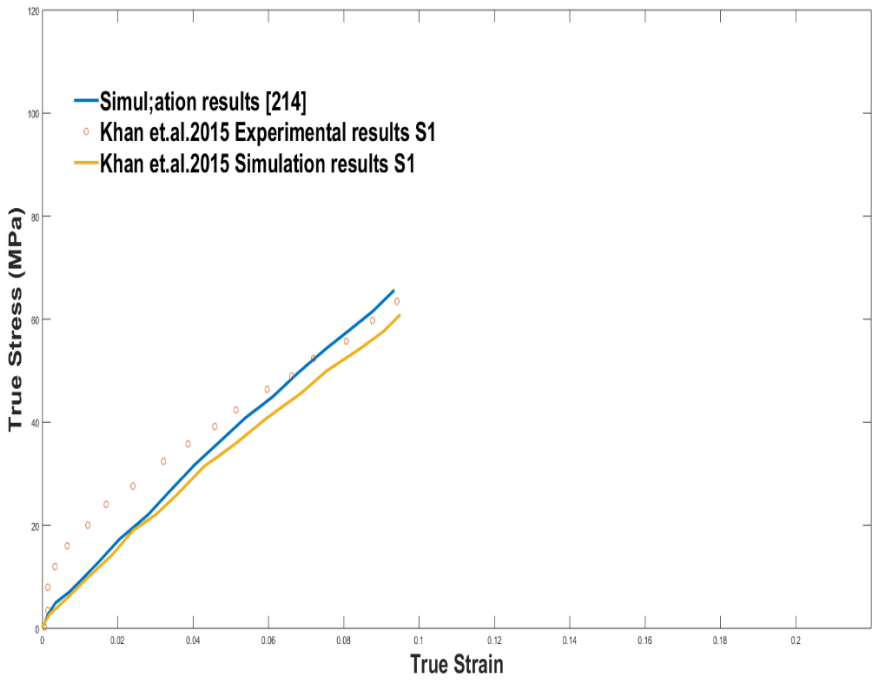

Fig 3.9: Stress-Strain curves of single crystal with orientation S1 at a strain rate of 1000/s

The stress strain curve for single slip corresponding to the high rate of deformation is presented in the Figure 3.10. The simulation curve has an initial bump corresponding to the elastic limit & it shows some significant deviation from the experimental curve in the middle part of stretching and then it starts to converge with the experimental plot. The curves produced by Khan et al. [2015] has similar deviation to the experimental but has slightly more convergence .

In all, the simulation curve of this study underestimate in the middle and overestimate latter on.

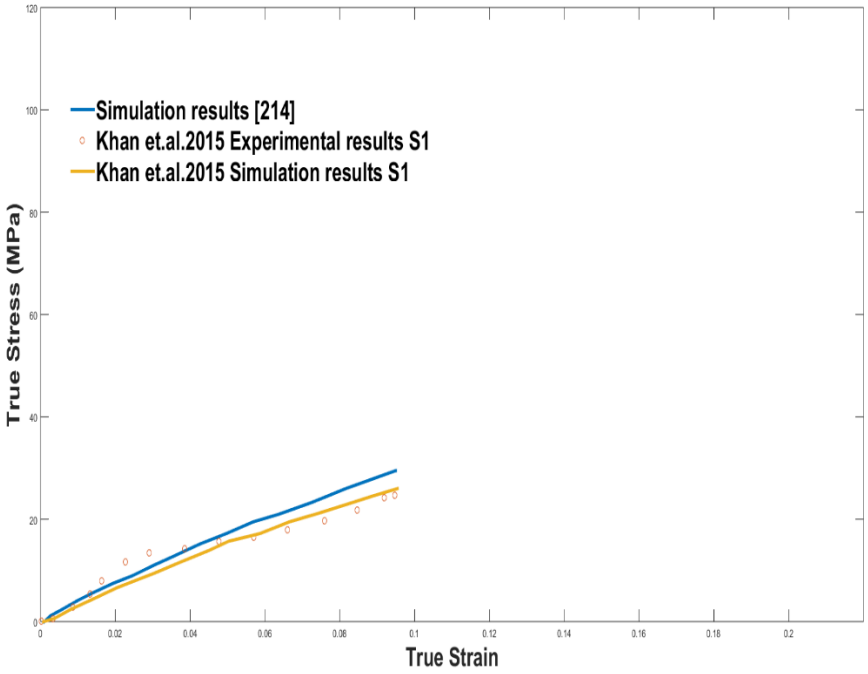

Fig.3.10: Stress-Strain curves of single crystal with orientation S1 at a strain rate of 0.001/s

Chapter 4 Numerical Implementation for Aluminium bicrystals

4.1 Introduction

In this chapter , we are going to implement our model to the Aluminium bicrystals to understand the deformation mechanism when there are more than one crystals (grains) and how do orientation of one grain relative to another effects the Plastic deformation so we will analyze the generated contour plot as well . The grain boundaries serve as obstacles to the motion of dislocations, causing them to pile up at the boundary resulting in a stress concentration that increases the required stress for activation of dislocation sources.

Firstly, we will extend our model to single element single grain to single element bicrystal and then we will extend it to multi element bicrystal and the generated contour plot would be analyzed.

4.2 Contour Plot and Stress- Strain curve for single element (bicrystal):

The input parameters and the boundary conditions will be taken the same as discussed in the section of One element test of single Al crystal so one can refer the section for the input and the boundary conditions. Here we will present the contour plot and the stress-strain curve for single element bicrystal under multi-slip mode for strain rate approximately ~ 0.001/s. Regarding the grain orientation of two grains, we used are as follows:

Grain ID	Grain orientation (Euler Angles)		
1	101.98	145.03	249.44
2	30.42	149.53	2.60

Table 4.1: Grain orientations of the two grains used to study the bicrystal.

Firstly from the simulation for single element single grain as carried out in the third chapter is extended to single element two grains so that we verify that input file and the user material subroutine is properly collaborated well with and the texture file as created by us . The following

page shows the contour plot of single element bicrystals followed by it's corresponding stress-strain curve is given.

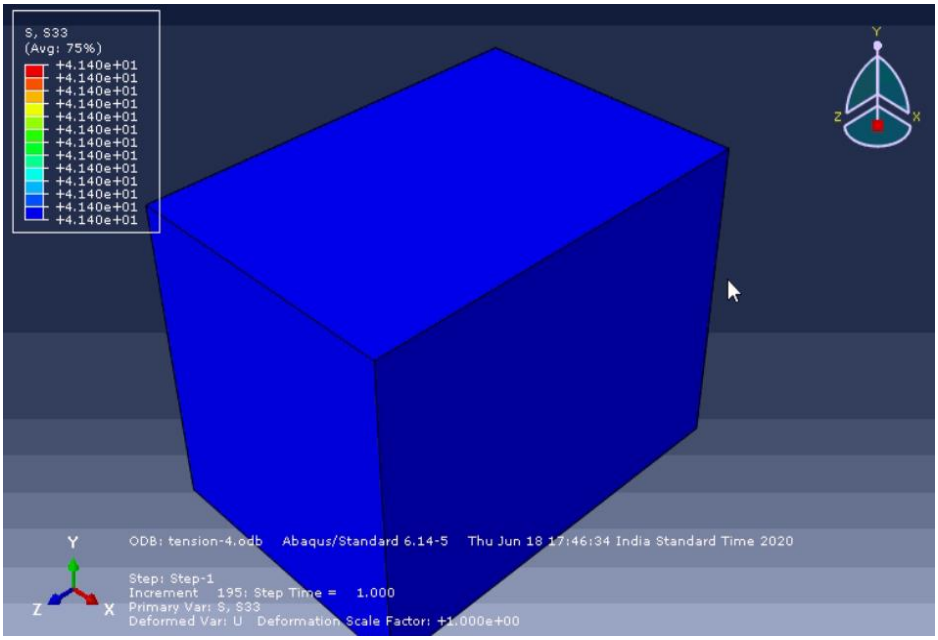

Figure 4.1 : Contour plot of single element bicrystals loaded in the z-direction.

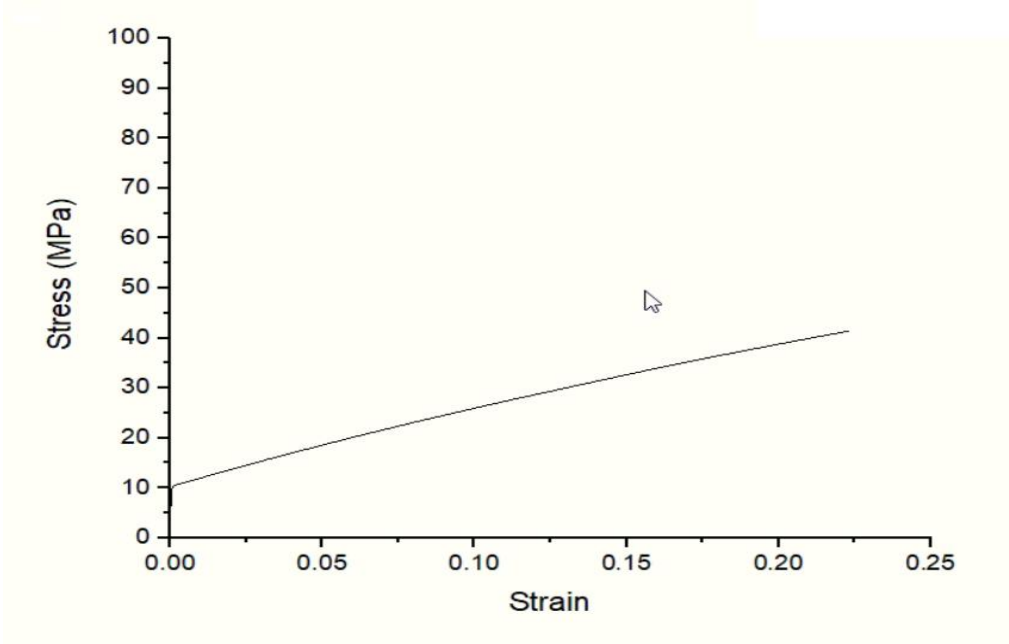

Figure 4.2 Stress- strain curve for single element bicrystals for strain rate of approximately ~ 0.001/s

The grain orientations are taken from the data of grain orientation of Ma et al. study of Aluminum polycrystals [2009]. The grain boundary thickness is assumed to be negligible compared to any element of the multi element simulation.

The top half of the elements consists of grain id1 orientation whereas the bottom half of the elements consists of grain id 2 orientation. As can be seen in the contour plots, there is deviation of stress values of various elements of different grains.

Also, there has been an increase in the average (von-mises) stress in all the elements indicating the effect of different grain orientation has been posing an additional resistance to the dislocation motion.

4.3 Contour Plot and Stress- Strain curve for multiple element (bicrystal) :

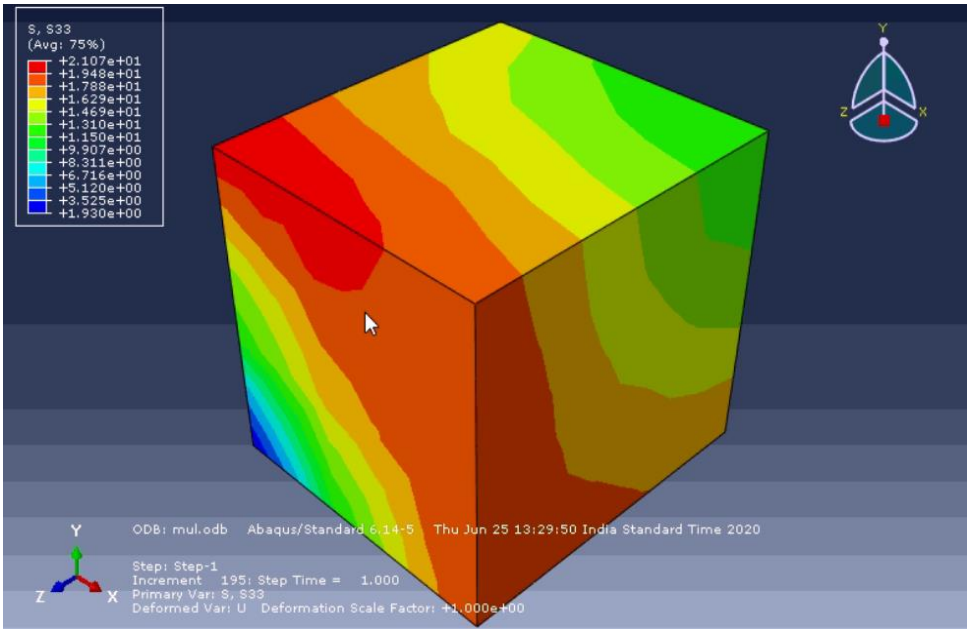

Figure 4.3a) : Contour plot of multi- elements bicrystals loaded in the z-direction (top half represents one grain and the bottom half represents the second grain at 5% strain)

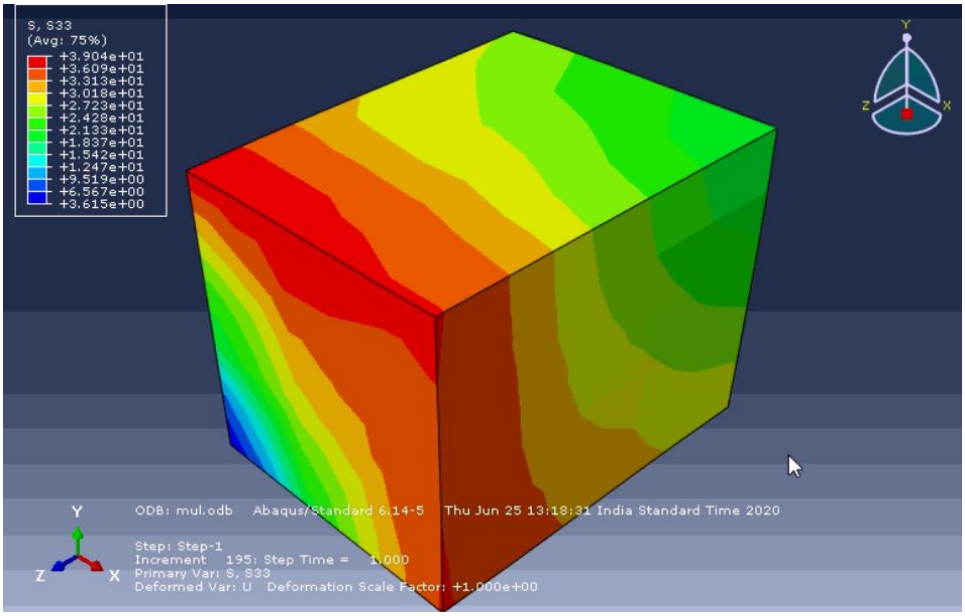

Figure 4.3 b) : Contour plot of multi- elements bicrystals loaded in the z-direction (top half represents one grain and the bottom half represents the second grain at 15% strain).

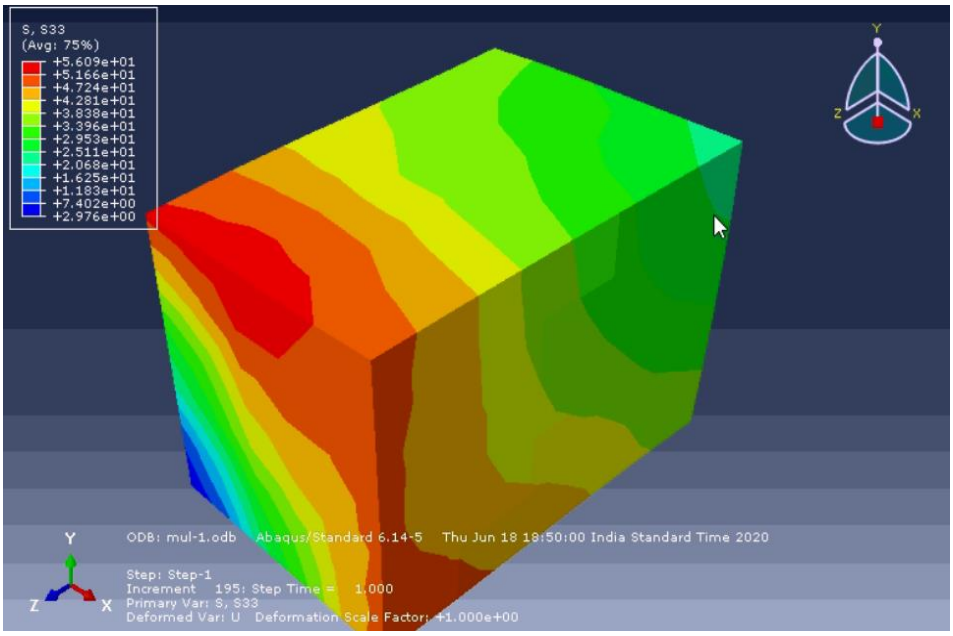

Figure 4.3 c) : Contour plot of multi- elements bicrystals loaded in the z-direction (top half represents one grain and the bottom half represents the second grain at 25% strain).

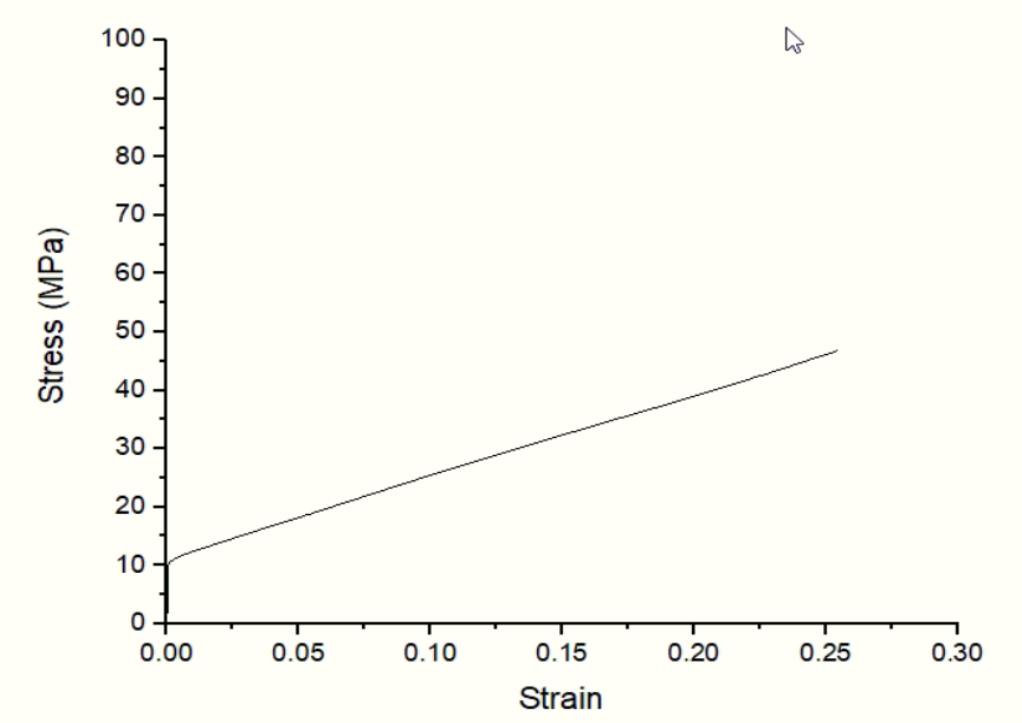

Figure 4.4a) Stress- strain curve for multiple element bicrystals for strain rate of approximately ~ 0.001/s

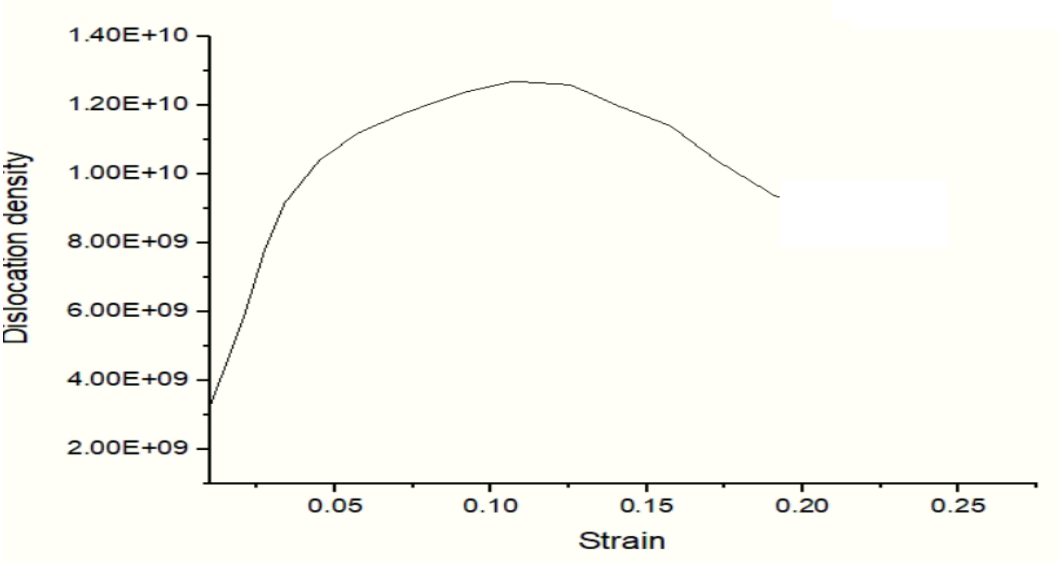

Figure 4.4 b) Variation of Dislocation density (m^{-2}) of the element near the grain boundary

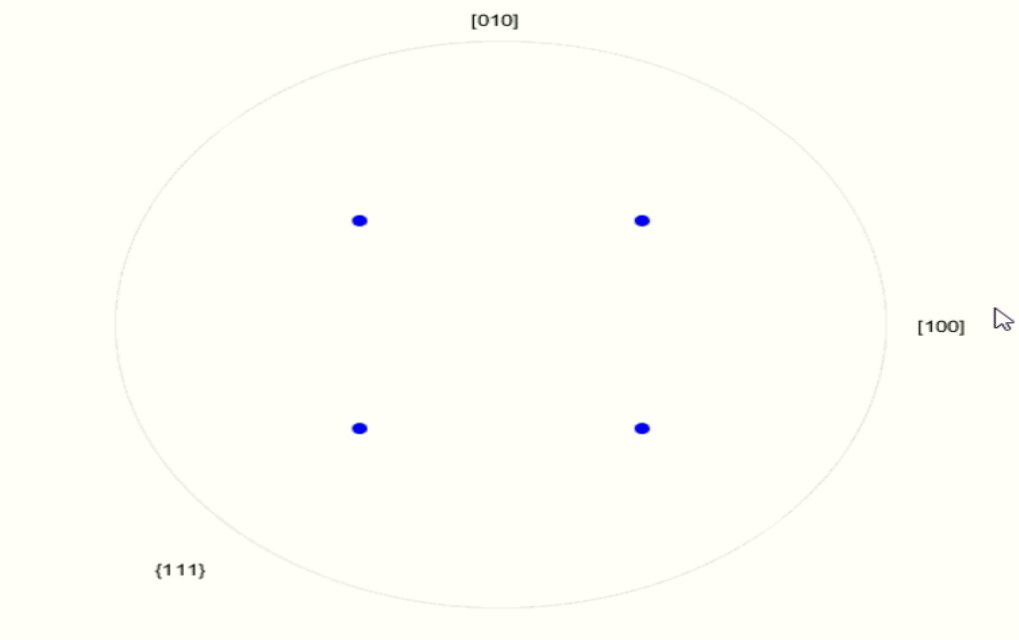

Figure 4.4 c) Pole Figure of the Aluminium bicrystals after the end of plastic deformation .

State of bicrystals	Fully Active	Mostly active	Moderately active	Marginally active	Almost inactive
At 5% plastic strain	3, 4, 9 ,10	None	6	6 , 7	1 , 2 ,5 ,8 11 , 12
At 15% plastic strain	3 , 4	9, 10	8	1,2 , 6, 7	5,8,11,12
At 25% plastic strain	3,4 , 9 , 10	9 , 10	6	1,2	5,7,8,6,11,12

Figure 4.4 d) Information about the slip system activity for the element at the grain boundary

Thus, in this chapter we carried out the multi-element simulation of aluminium bicrystals to see the effect of different grain orientation. And, for that we have to create an additional texture file to be used for the simulation works. Beside the simulation resulted in the texture files in the output One can use this file to plot any pole figures and calculate orientation distribution functions (ODFs) using the texture software MTEX (a MATLAB tool box).

Serial No.	Slip System
1	$(1\ 1\ 1)\ [\bar{1}\ 0\ 1]$
2	$(1\ 1\ 1)\ [\bar{1}\ 1\ 0]$
3	$(1\ 1\ 1)\ [0\ \bar{1}\ 1]$
4	$(\bar{1}\bar{1}\ 1)\ [0\ 1\ 1]$
5	$(\bar{1}\bar{1}\ 1)\ [\bar{1}\ 1\ 0]$
6	$(\bar{1}\bar{1}\ 1)\ [1\ 0\ 1]$
7	$(\bar{1}\ 1\ 1)\ [1\ 0\ 1]$
8	$(\bar{1}\ 1\ 1)\ [1\ 1\ 0]$
9	$(\bar{1}\ 1\ 1)\ [0\ \bar{1}\ 1]$
10	$(1\ \bar{1}\ 1)\ [0\ 1\ 1]$
11	$(1\ \bar{1}\ 1)\ [1\ 1\ 0]$
12	$(1\ \bar{1}\ 1)\ [\bar{1}\ 0\ 1]$

Table 4.2: Various slip system numbered in FCC crystals referred in this section .

In this work we have not carried out the texture evolution related study, the scope of such works is mentioned in the Concluding remarks.

Chapter 5 Concluding remarks

5.1 Concluding remarks and future scope of this work

The constitutive description and computational implementation of a rate independent constitutive model for single crystal plasticity is not only an interesting problem but also a challenging one. The main obstacle encountered in the computational implementation of the crystal plasticity model, is to get the stress increment algorithm to converge and at the same time not affecting the inner newton-raphson algorithm. The problem was solved using extensive debugging of the developed UMAT.

In this work we were concerned with the formulation of a rate dependent constitutive model for single crystal plasticity, combining elementary concepts from material's science and continuum mechanics. We presented a developed stress–increment algorithm. A modified hardening model was also introduced to incorporate the effects of dislocation density and make the model more physics based. A series of finite element simulations were conducted on both single and multi-finite element models, in an effort to investigate the effects of, crystal orientation rate of deformation on the plastic behavior of FCC metal single crystals and then latter on the bicrystals. Computationally, we also performed a comparison between experimental results obtained in the literature and the one shown by Khan et al. [2015].

Several research directions may be proposed for future work, all of which aim to the development of a robust, comprehensive and computationally implementable crystal plasticity model. A problem of particular interest would be to study the later stages of hardening and usage of different expressions for hardening to match or approximate the physics of plastic deformation in FCC crystals. Also, one can use such physics-based modeling laws on the other crystalline structures as well. Another interesting project would be to computationally investigate the behavior of single crystal materials that are subjected into complex loading conditions. To this end, an intriguing project would be to study the fracture behavior of single crystals and study the effect of various complex shaped notches and their geometries in the deformation behavior of crystalline materials .

Ultimately, all aforementioned research directions are motivated by the need for a robust crystal plasticity model that would be able to perform realistic predictions, be in agreement with the experimental observations and also simulate the effect of various parameters (i.e. strain rate, geometric discontinuities, complex loading conditions) to the plastic behavior of single crystals and polycrystals (Bicrystals being the special case).

Appendix

A.1 Results and discussions on Copper single crystal

The model discussed in this work when applied on the Cu single crystal is fitted firstly with the experimental results obtained in the literature (Taguchi,1974) in the direction [-1 2 3] as done by Lee et al. [2010] and then compared with the dislocation density model given by Lee et al.[2010]

Orientations	ρ^{α}	y_c	**K**	γ_0^{α}	a_0
[321]	10^{10}	15.0E-10	42	1.73E6	0.08
[211]	10^{10}	15.0E-10	42	1.73E6	0.08
[111]	10^{10}	15.0E-10	42	1.73E6	0.08
[100]	10^{10}	04.0E-10	42	1.73E6	0.08

Table 5.1: Fitted parameters of Cu single crystal with the experimental results of Taguchi [1974]

It can be observed that the dislocation density-based model used in this study is deviating or in other words overly estimating in the first two orientations of the following figure and underestimating the experimental results in the latter two orientations. But at the same time the results of Lee el al. [2009] have even more mismatch compared to the results produced by this study whereas matching reasonably well with the experimental results of the first two orientations.

In essence this is partly due to multi slip being pronounced more heavily in the latter two orientations as can also be seen in the stereographic triangle .The reader might question seeing the plots being one being engineering stress – strain curve and other being true stress strain but the plots with which they are compared are of same nature and hence the comparison being valid to look at and infer from .

The future scope of this small auxiliary can be to investigate the reasons behind the mismatch and develop more experimentally capturing models i.e., the models which captures the physics of plastic deformation in slightly better way than ours.

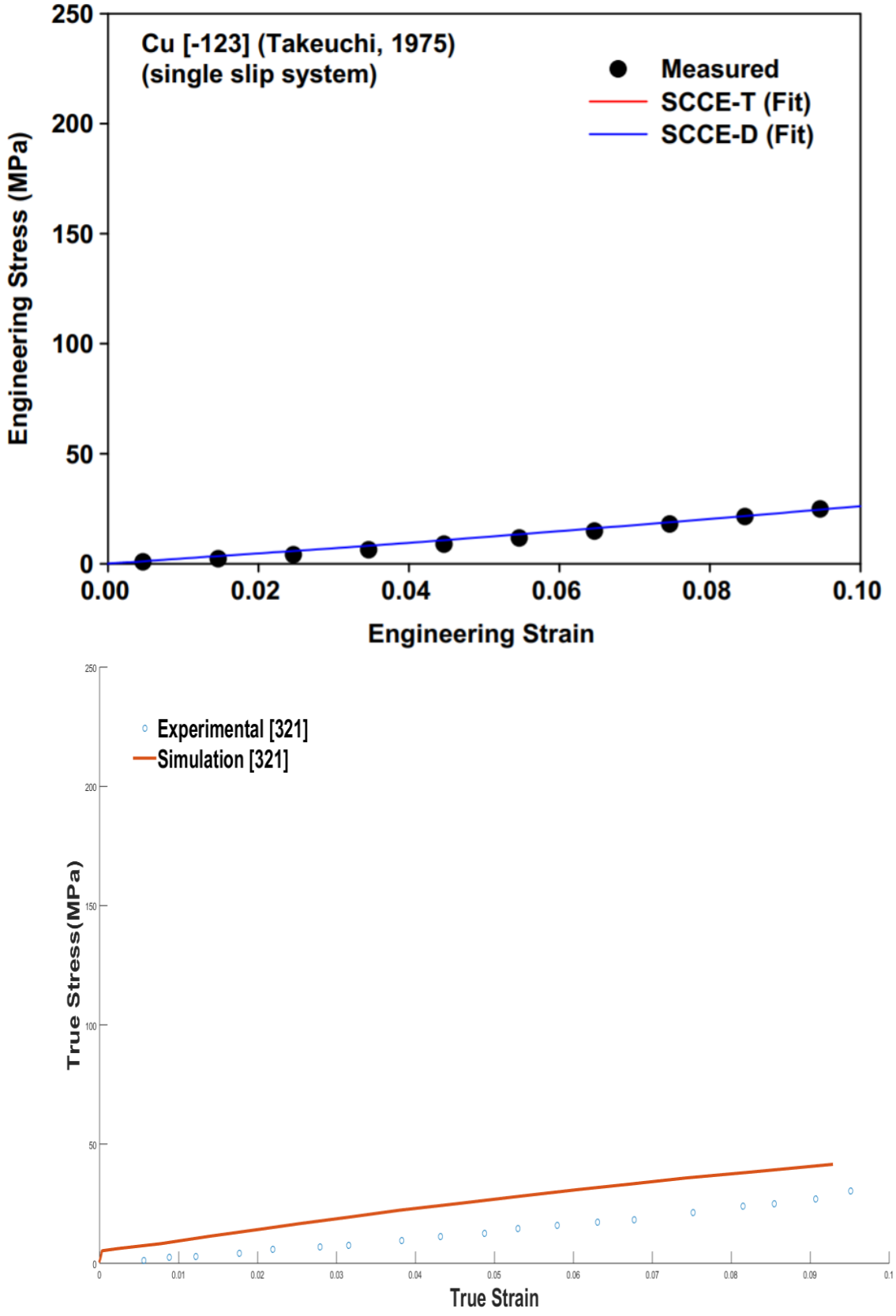

Figure A.1: Comparison of simulation and experimental results of Cu single crystal in the orientation [321]

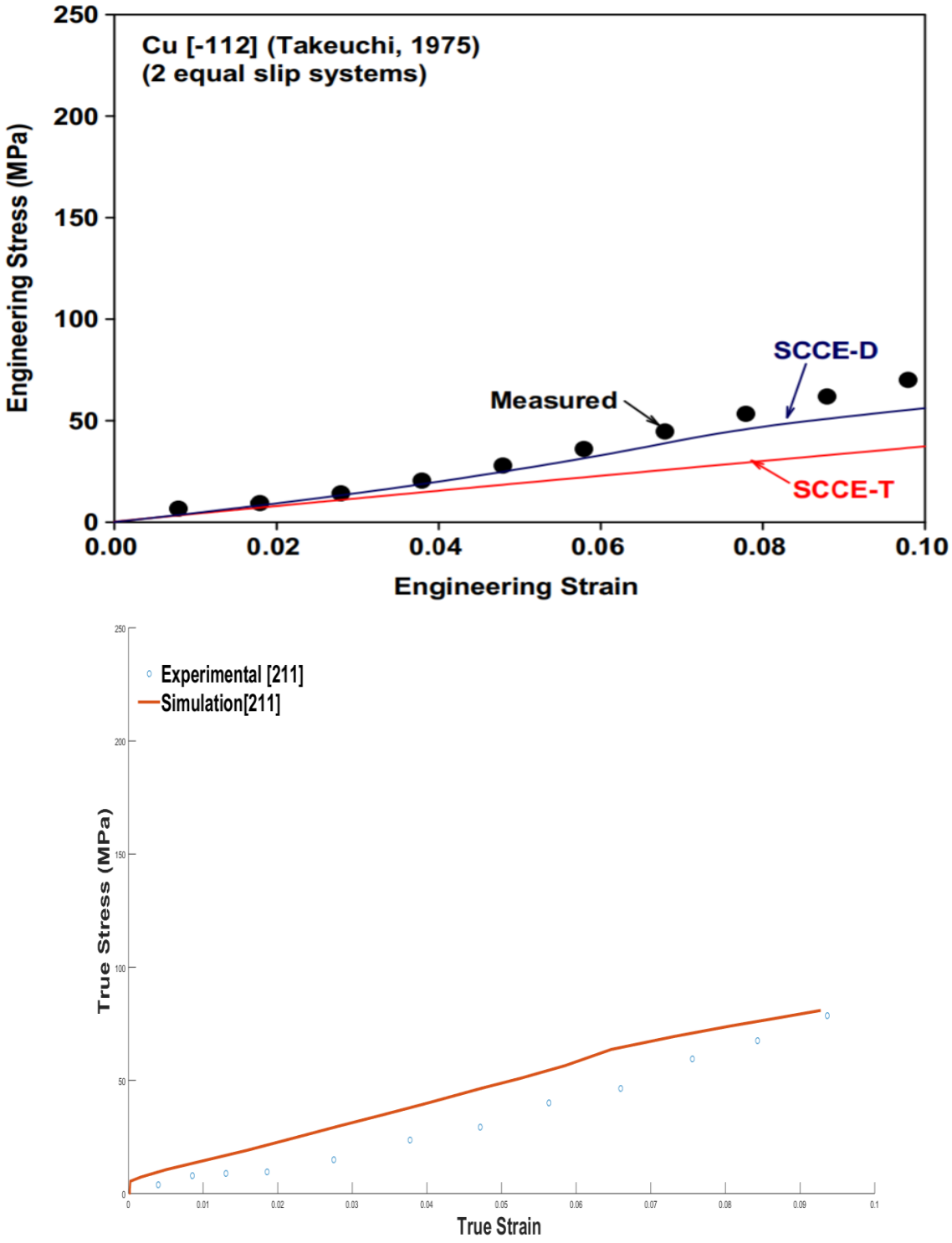

Figure A.2: Comparison of simulation and experimental results of Cu single crystal in the orientation [-112]

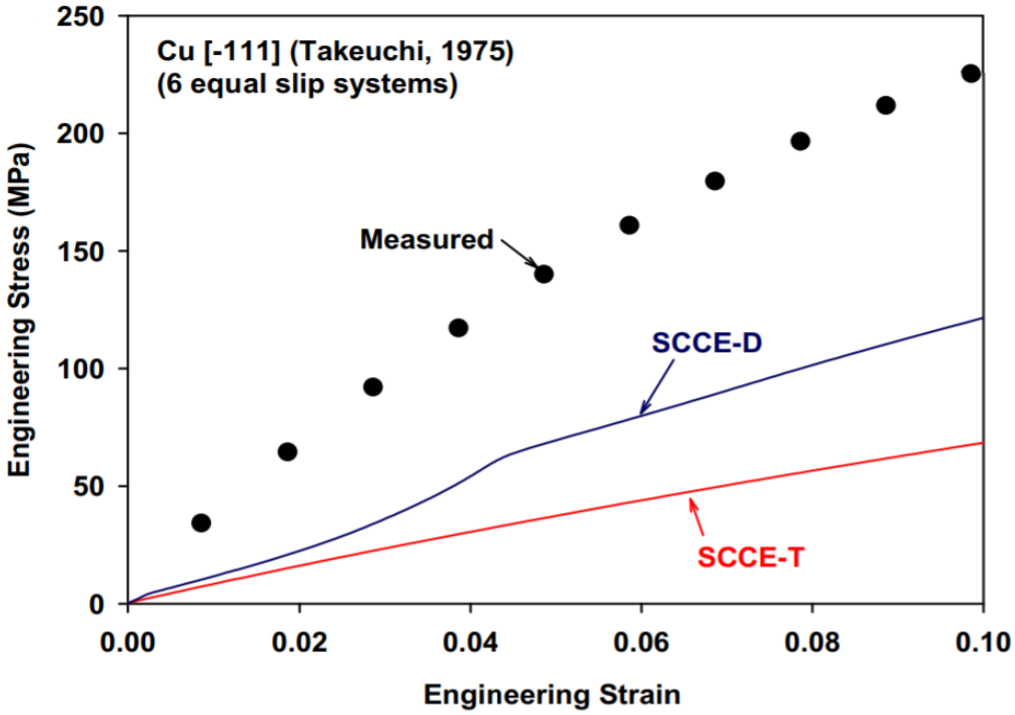

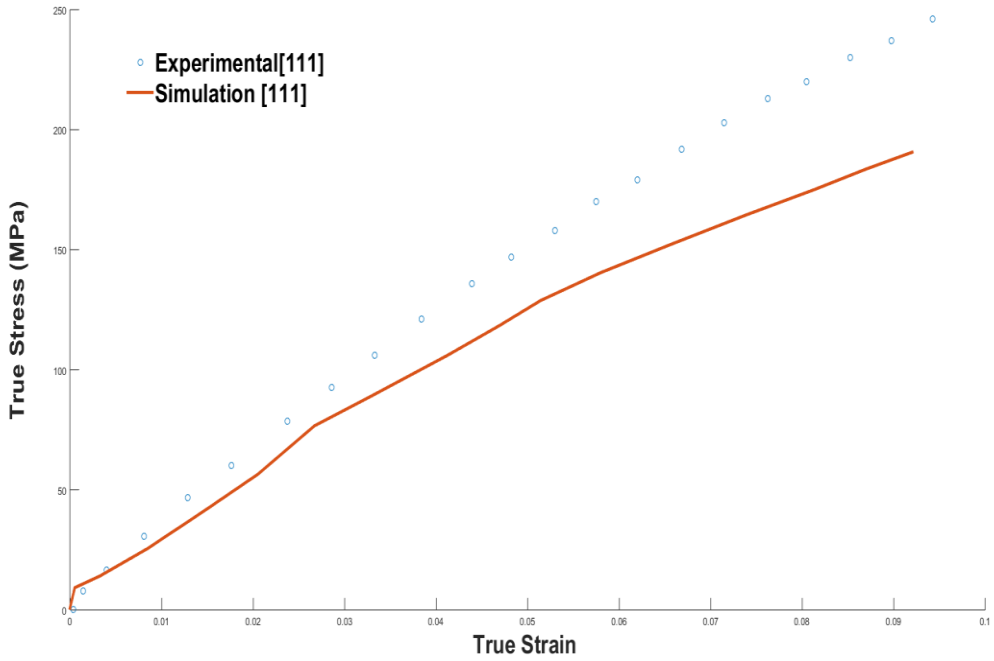

Figure A.3 Comparison of simulation and experimental results of Cu single crystal in the orientation [111]

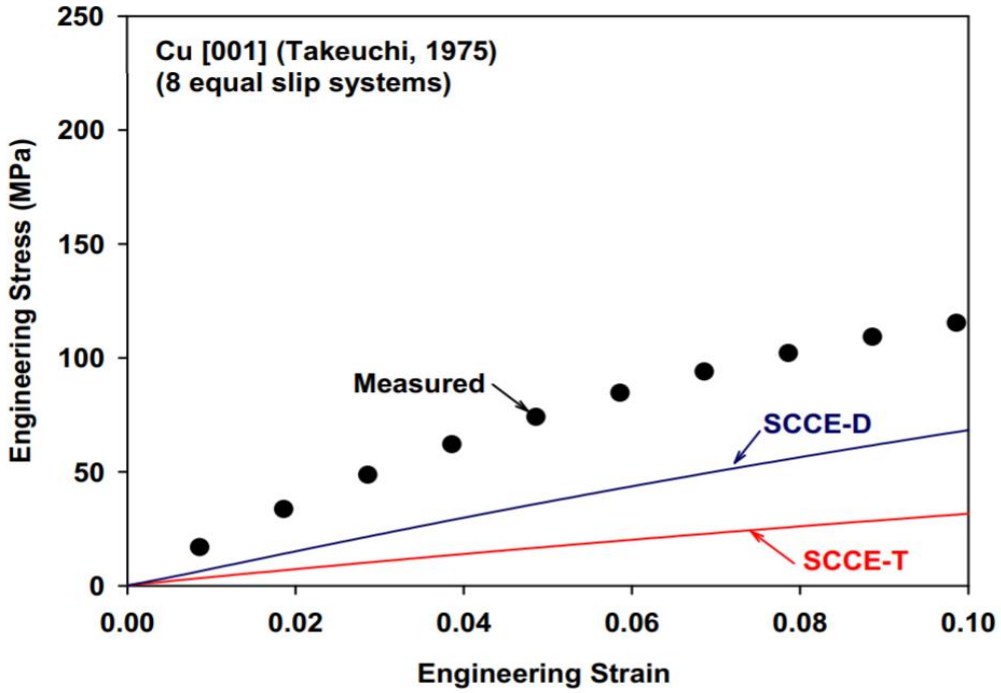

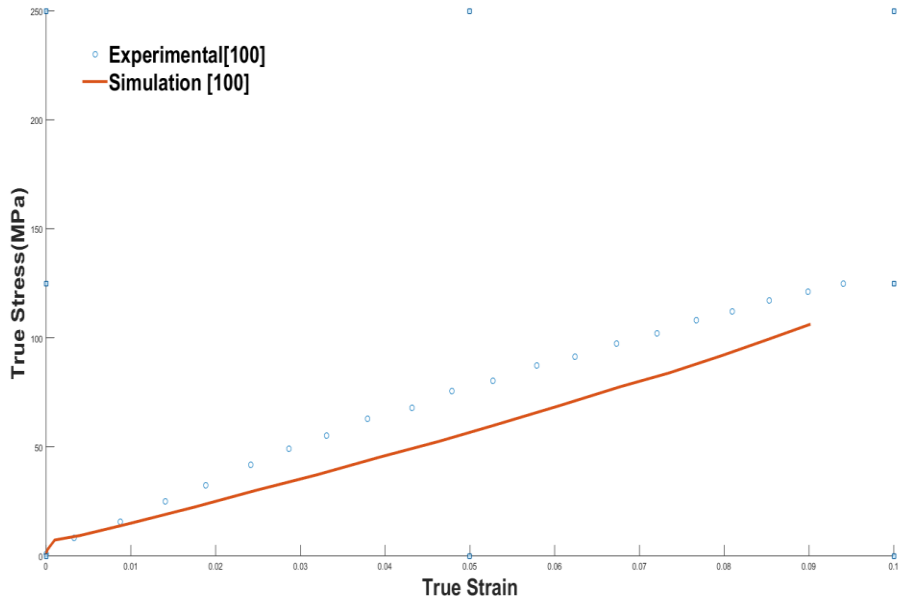

Figure A.4 Comparison of simulation and experimental results of Cu single crystal in the orientation [100]

References

[ABAQUS, 2017] Hibbit, Karlson and Sorenson Inc., Providence, R. I. ABAQUS, Reference Manuals, 1993.

[Anand, 1985] L. Anand. Constitutive equations for hot-working of metals. International Journal of Plasticity, 1:213-231, 1985.

[Asaro and Needleman, 1985] R. J. Asaro and A. Needleman. Texture development and strain hardening in rate dependent polycrystals. Acta Metallurgica, 33:923-953, 1985.

[Barlat et al., 1991b] F. Barlat, S. Panchanadeeswaran, and 0. Richmond. Earing in cup drawing face-centered cubic single crystals and polycrystals. Metallurgical Transactions. A., 22:1525-1534, 1991b.

[Bassani and Wu, 1991] J. L. Bassani and T. Y. Wu. Latent hardening in single crystals (ii). analytical characterizations and predictions. Proceedings of the Royal Society of London, A 435:21-41, 1991.

[Bassani, 1993] J. L. Bassani. Plastic flow of crystals. Advances in Applied Mechanics, 30:191-254, 1993. [Becker et al., 1993] R. Becker, R. E. Smelser, and S. Panchanadeeswaran. Simulations of earing in aluminium single crystals and polycrystals. Modelling and Simulations in Materials Science and Engineering, 1:203-224, 1993.

Barlat, F., Glazov, M.V., Brem, J.C., Lege, D.J., 2002. A simple model for dislocation behavior, strain and strain rate hardening evolution in deforming aluminum alloys. Int. J. Plast. 18, 919–939.

Bassani, J.L., Wu, T.-Y., 1991. Latent hardening in single crystals II. Analytical characterization and predictions. Proc.: Math. Phys. Sci. 435, 21–41. Becker, R., 1991.

Analysis of texture evolution in channel die compression—I. Effects of grain interaction. Acta Metall. Mater. 39, 1211–1230.

J. Bell, J.F., Green, R.E., 1967. An experimental study of the double slip deformation hypothesis for face-centred cubic single crystals. Philos. Mag. 15, 469–476

Beyerlein, I.J., Tomé, C.N., 2007. Modeling transients in the mechanical response of copper due to strain path changes. Int. J. Plast. 23, 640–664

. Beyerlein, I.J., Tomé, C.N., 2008. A dislocation-based constitutive law for pure Zr including temperature effects. Int. J. Plast. 24, 867–895.

Bronkhorst, C.A., Kalidindi, S.R., Anand, L., 1992. Polycrystalline Plasticity and the Evolution of Crystallographic Texture in FCC Metals. Philos. Trans. Phys. Sci. Eng. 341, 443–477. Carreker, R., Hibbard, W., 1957. Tensile deformation of aluminum as a function of temperature, strain rate, and grain size. Trans. AIME 209, 1157–1163. Cottrell, A.H., Stokes, R.J., 1955. Effects of temperature on the plastic properties of aluminium crystals. Proc. Roy. Soc. Lond. Ser. A. Math. Phys. Sci. 233, 17– 34.

Edington, J.W., 1968. Effect of strain rate on the dislocation substructure in deformed niobium single crystals. In: Lindholm, U.S. (Ed.), Mechanical Behavior of Materials under Dynamic Loads. Springer, Berlin Heidelberg, pp. 191–240.

Estrin, Y., Tóth, L.S., Molinari, A., Bréchet, Y., 1998. A dislocation-based model for all hardening stages in large strain deformation. Acta Mater. 46, 5509– 5522

Farrokh, B., Khan, A., 2009. Grain size, strain rate, and temperature dependence of flow stress in ultra-fine grained and nanocrystalline Cu and Al: synthesis, experiment, and constitutive modeling. Int. J. Plast. 25, 715–732

Ferguson, W.G., Hauser, F.E., Dorn, J.E., 1967. Dislocation damping in zinc single crystals. Brit. J. Appl. Phys. 18, 411

. Franciosi, P., Zaoui, A., 1982. Multislip in f.c.c. crystals a theoretical approach compared with experimental data. Acta Metall. 30, 1627–1637

Gurtin, M.E., 2010. A finite-deformation, gradient theory of single-crystal plasticity with free energy dependent on the accumulation of geometrically necessary dislocations. Int. J. Plast. 26, 1073–1096.

Special Issue in Honor of Lallit Anand. Hansen, B.L., Beyerlein, I.J., Bronkhorst, C.A., Cerreta, E.K., Dennis-Koller, D., 2013. A dislocation-based multi-rate single crystal plasticity model. Int. J. Plast. 44, 129–146.

Harren, S.V., Asaro, R.J., 1989. Nonuniform deformations in polycrystals and aspects of the validity of the Taylor model. J. Mech. Phys. Solids 37, 191–232. http://dx.doi.org/10.1016/0022-5096(89)90010-0. Harren, S.V., Dève, H.E., Asaro, R.J., 1988. Shear band formation in plane strain compression. Acta Metall. 36, 2435–2480

Hill, R., 1965. Continuum micro-mechanics of elastoplastic polycrystals. J. Mech. Phys. Solids 13, 89–101.

Hill, R., Rice, J.R., 1972. Constitutive analysis of elastic-plastic crystals at arbitrary strain. J. Mech. Phys. Solids 20, 401–413

Hosford Jr., W., Fleischer, R., Backofen, W., 1960. Tensile deformation of aluminum single crystals at low temperatures. Acta Metall. 8, 187–199.

Howe, S., Liebmann, B., Lücke, K., 1961. High temperature deformation of aluminum single crystals. Acta Metall. 9, 625–631

Huang, Y., 1991. A User-Material Subroutine Incorporating Single Crystal Plasticity in the ABAQUS Finite Element Program. Mech Report 178, Division of Applied Sciences, Harvard University, Cambridge, MA. Hutchinson, J.W., 1976. Bounds and self-consistent estimates for creep of polycrystalline materials. Proc. Roy. Soc. Lond. A. Math. Phys. Sci. 348, 101–127

Khan, A.S., Liang, R., 1999. Behaviors of three BCC metal over a wide range of strain rates and temperatures: experiments and modeling. Int. J. Plast. 15, 1089–1109.

Khan, A., Zhang, H., Takacs, L., 2000. Mechanical response and modeling of fully compacted nanocrystalline iron and copper. Int. J. Plast. 16, 1459–1476. Khan, A., Suh, Y., Kazmi, R., 2004. Quasi-static and dynamic loading responses and constitutive modeling of titanium alloys. Int. J. Plast. 20, 2233–2248.

Khan, A., Kazmi, R., Farrokh, B., Zupan, M., 2007. Effect of oxygen content and microstructure on the thermo-mechanical response of three Ti–6Al–4V alloys: experiments and modeling over a wide range of strain-rates and temperatures. Int. J. Plast. 23, 1105–1125

Knezevic, M., McCabe, R.J., Lebensohn, R.A., Tomé, C.N., Liu, C., Lovato, M.L., Mihaila, B., 2013a. Integration of self-consistent polycrystal plasticity with dislocation density based hardening laws within an implicit finite element framework: application to low-symmetry metals. J. Mech. Phys. Solids 61, 2034–2046.

Knezevic, M., Lebensohn, R.A., Cazacu, O., Revil-Baudard, B., Proust, G., Vogel, S.C., Nixon, M.E., 2013b. Modeling bending of a-titanium with embedded polycrystal plasticity in implicit finite elements. Mater. Sci. Eng.: A 564, 116–126

Knezevic, M., McCabe, R.J., Tomé, C.N., Lebensohn, R.A., Chen, S.R., Cady, C.M., Gray III, G.T., Mihaila, B., 2013c. Modeling mechanical response and texture evolution of a-uranium as a function of strain rate and temperature using polycrystal plasticity. Int. J. Plast. 43, 70–84

Knezevic, M., Beyerlein, I.J., Brown, D.W., Sisneros, T.A., Tomé, C.N., 2013d. A polycrystal plasticity model for predicting mechanical response and texture evolution during strain-path changes: application to beryllium. Int. J. Plast. 49, 185–198

Knezevic, M., Drach, B., Ardeljan, M., Beyerlein, I.J., 2014. Three dimensional predictions of grain scale plasticity and grain boundaries using crystal plasticity finite element models. Comput. Methods Appl. Mech. Eng. 277, 239–259.

Kocks, U.F., Mecking, H., 2003. Physics and Phenomenology of Strain Hardening: The FCC Case. Pergamon. Kröner, E., 1959. Allgemeine Kontinuumstheorie der Versetzungen und Eigenspannungen. Arch. Ration. Mech. Anal. 4, 273–334.

.Kubin, L.P., Estrin, Y., 1990. Evolution of dislocation densities and the critical conditions for the Portevin-Le Châtelier effect. Acta Metall. Mater. 38, 697–708

Lebensohn, R.A., Tomé, C.N., 1993. A self-consistent anisotropic approach for the simulation of plastic deformation and texture development of polycrystals: application to zirconium alloys. Acta Metall. Mater. 41, 2611–2624.

K. Lee, W.B., Chen, Y.P., 2010. Simulation of micro-indentation hardness of FCC single crystals by mechanism-based strain gradient crystal plasticity. Int. J. Plast. 26, 1527–1540.

Lee, M.G., Lim, H., Adams, B.L., Hirth, J.P., Wagoner, R.H., 2010. A dislocation density-based single crystal constitutive equation. Int. J. Plast. 26, 925–938

Les, P., Zehetbauer, M., Stüwe, H.P., 1996. Characteristics of work hardening in late stages of high temperature deformation of aluminium single crystals. Phys. Stat. Sol. (a) 157, 265–273.